FLUORESCENT MOLECULAR ROTORS AS

MECHANOSENSORS IN BIOFLUIDS

A Dissertation

presented to

the Faculty of the Graduate School

University of Missouri-Columbia

In Partial Fulfillment

Of the Requirements for the Degree

Doctor of Philosophy

---

by

WALTER JOHN AKERS

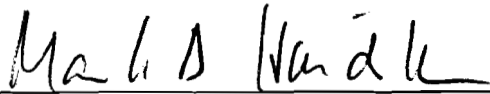Dr. Mark A. Haidekker, Dissertation Supervisor

DECEMBER 2005

The undersigned, appointed by the Dean of the Graduate School, have examined the dissertation entitled.

FLUORESCENT MOLECULAR ROTORS AS

MECHANOSENSORS IN BIOFLUIDS

Presented by Walter John Akers

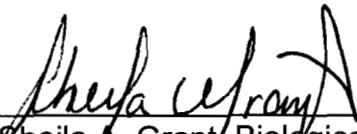A candidate for the degree of Doctor of Philosophy

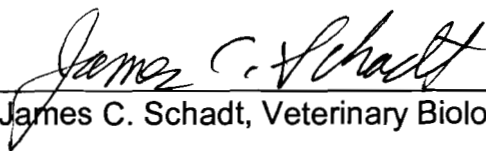And hereby certify that in their opinion it is worthy of acceptance.

Mark A. Haidekker, Biological Engineering

Allen W. Hahn, Veterinary Medicine

Sheila A. Grant, Biological Engineering

James C. Schadt, Veterinary Biological Sciences

Kevin Gillis, Biological Engineering

DEDICATION

This work is dedicated to:

my Lord and Savior, Jesus Christ who has blessed me more than I could ever deserve;

my wife, Renee, for the boundless love and support she has given me since the day we met and especially during the time it took to complete this work;

all my family and friends through my life who have helped me to become the person I am;

the members of my dissertation committee, Mark Haidekker, Kevin Gillis, Sheila Grant, Allen Hahn and James Schadt, have generously given their time and expertise to better my work.

ACKNOWLEDGMENTS

TABLE OF CONTENTS

LIST OF FIGURES

x

LIST OF TABLES

LIST OF ABBREVIATIONS

mPa s = milliPascal seconds

RBC = Red blood cell

UV = Ultraviolet

S_1 = Lowest energy excited state

S_0 = Ground energy state

т = Fluorescence lifetime

MW = Molecular weight

LED = Light-emitting diode

TICT = Twisted internal charge transfer

DCVJ = 9-(dicyanovinyl)-julolidine

HES = Hydroxyethyl starch

CCVJ = 9-[(2-Cyano-2-hydroxy carbonyl)vinyl]julolidine

DMSO = Dimethyl Sulfoxide

CCVJ-TEG = CCVJ-triethylene glycol ester

BSA = Bovine serum albumin

Diol = p-[(2-cyano-2-propanediol ester)vinyl]dimethylaniline

CCVJ-DEG = CCVJ-diethylene glycol ester

CCVJ-NHS = CCVJ-succimidyl ester

CCVJ-TEG-NHS = CCVJ-TEG-succimidyl ester

FLUORESCENT MOLECULAR ROTORS AS MECHANOSENSORS IN BIOFLUIDS

Walter J. Akers

Dr. Mark A. Haidekker, Dissertation Supervisor

ABSTRACT

Many disease states have associated blood viscosity changes. Molecular rotors, fluorescent molecules with viscosity sensitive quantum yields, have recently been investigated as a new method for biofluid viscosity measurement. Biofluid viscosity measurements by conventional methods are complicated by protein adherence to surfaces and formation of air-surface layers. The presented work demonstrates the usefulness of fluorescence viscometry using molecular rotors dissolved in aqueous solutions and blood plasma. The precision of fluorescence viscometry is compared with that of a state-of-the-art cone and plate viscometer. The interaction of molecular rotors in solution with blood plasma proteins is reported. The viscosity sensitivity of surface-immobilized molecular rotors to glass nanoparticles and optical fibers is also investigated. Conclusions: fluorescence viscometry using molecular rotors promises to be a powerful new method for biofluid viscosity measurement, delivering fast readout for microliter volume samples.

CHAPTER 1.

INTRODUCTION

1.1. Viscosity

On a macroscopic scale, viscosity of a fluid is its resistance to shear. Physical viscosity is defined by the ration of fluid shear stress to shear rate. The Debye-Stokes-Einstein (DSE) hydrodynamic model describes viscosity in relation to molecular size. The latter model assumes molecules to be spherical and does not account for frictional interactions that result from the electrostatic character of molecules and non-ideal shape.

Viscosity is caused by "cohesive forces" between molecules and the resulting friction as they pass each other. Every molecule has such a "force field" made up of attractive and repulsive forces such as charge, dielectric effects and van der Waal's forces. Intermolecular attractions are distance-dependent and can be estimated from the free space between molecules. This space decreases with temperature and with molecular size, as does viscosity [12]. Doolittle derived the equation for liquid viscosity in terms of solvent free volume [12].

$$\eta = A\exp(\frac{V_0}{V_f}) \qquad \textbf{(1)}$$

where A is a constant, V_0 is the van der Waals volume and V_f is the free volume of the solvent [41]. Doolittle showed that the relationship of molecular weight to viscosity of paraffins, and observed that at constant temperature could be

described by Eq. 1. It is difficult to calculate the exact forces present between

individual components of biofluids such as blood plasma because of their

complex composition, but the basic concepts are useful in rheology.

1.2. Blood Viscosity Measurement

Viscosity measurement today relies on determining the ratio of shear

stress τ to shear rate γ. Rheology is the study of fluid change during flow. The

Pascal-second (Pa s) is the SI unit for viscosity.

1.2.1. Cone and Plate Viscometer

The cone and plate viscometer (Fig. 1) measures the resistance to shear

of a fluid placed between a flat
stationary plate and rotating cone
of known angle α. For simple,
idealized flow, inertial effects must
be negligible, α must be small (<4
degrees), and the axis of rotation
perpendicular to plate surface [9].

Figure 1: Schematic of cone and plate viscometer.

Viscosity is measured with a cone
and plate viscometer using Eq. 2

$$\eta = \frac{3T\alpha}{2\pi R^3 \omega} \qquad \textbf{(2)}$$

where η is viscosity, α is the angle of the cone with respect to the plate, ω is angular velocity, and T is the torque on the spindle and is related to the surface area of the cone. The cone and plate viscometer produces constant shear rate and shear stress throughout the sample for Newtonian fluids.

1.2.2. Concentric-Cylinder Viscometer

The concentric-cylinder or Couette viscometer (Fig. 2) measures viscosity by shearing the fluid between two cylinders. The inner cylinder (bob) is immersed in the fluid and rotated at a constant angular velocity ω, while the outer cylinder is stationary. The total torque required to rotate the bob is related directly to fluid shear stress and viscosity by:

$$\eta = \frac{T(\kappa - 1)}{2\pi R^2 L \kappa^3 \omega} \qquad \textbf{(3)}$$
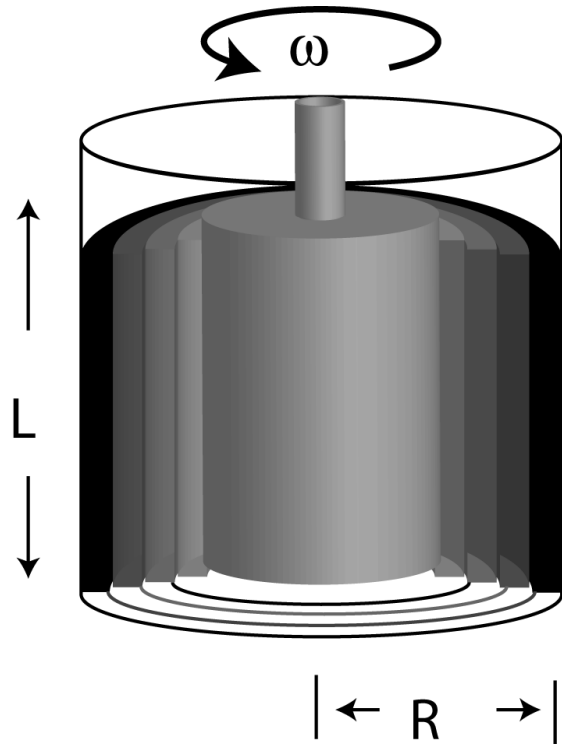
Figure 2: Couette (concentric cylinder) viscometer.

The Couette viscometer geometry allows measurement of low-viscosity fluids due to the large contact area of the bob. This geometry also allows sedimentation of particles in suspensions, which

is important for viscosity measurements of such fluids as blood.

1.2.3. Capillary Viscometer

Another instrument for fluid viscosity measurement is the capillary viscometer (Fig. 3). It operates on the principle of gravity-induced flow hindered by viscous forces. Viscosity can be determined according to Poiseuille's formula [58]:

$$\eta = \frac{\Delta P \pi r^4}{8LQ} \tag{4}$$

where ΔP is the change in pressure over the length of the capillary L, and at the fluid flow rate Q. Capillary viscometers to measure small sample volumes (<1 ml) have been developed, but
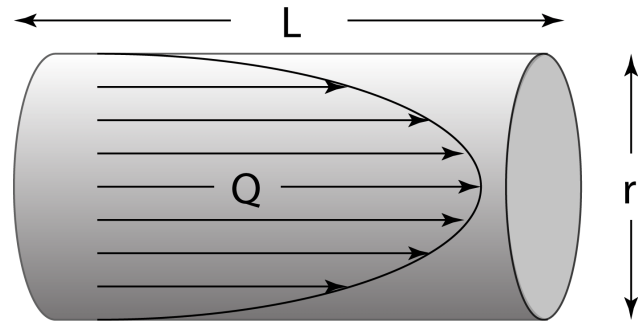
Figure 3: Schematic of a capillary viscometer.

large volumes (500 ml) are needed for high accuracy [58]. Capillary viscometers suffer from the same drawbacks as the cone-plate viscometer including long measurement and cleanup times and the application of shear to the fluid samples. Capillary viscometers are limited to viscosity measurement at high shear rates [49].

1.3. Importance of Blood Viscosity

Plasma proteins form a layer at the blood-air interface that gives blood plasma apparent non-Newtonian properties and inhibits accurate viscosity measurement [9]. In addition, protein adsorption to instrument surfaces may cause erroneous readings so that meticulous cleaning is required between samples. An instrument that could quickly and accurately measure viscosity of small quantities of blood, in succession, without applying shear would greatly benefit the study of blood rheology and its utilization in disease diagnosis and treatment.

It is difficult to determine the viscosity of whole blood using shear-dependent instruments due to "wall effects". Blood plasma forms a boundary layer between the smooth shearing surfaces and the red blood cells so that true viscosity is not measurable [9]. Red-cell sedimentation and aggregation at low shear rates also makes measurement difficult.

Abnormalities in blood viscosity are seen in many pathologic conditions such as diabetes mellitus [50,42], stroke, severe hemorrhage, hypertension [43] immunologic diseases and some cancers [38,65], [36,4]. Viscosity changes are also characteristic of nonpathologic conditions such as exercise, smoking, and age-related changes. "Hyperviscosity syndrome" covers a range of diseases characterized by increased blood viscosity [65]. Blood viscosity may increase because of increased cell content (polycythemia), decreased cell flexibility (scleracythemia), and elevated plasma protein concentration (paraproteinemia) [49]. Increased blood viscosity has been related to the occurrence and severity of

heart disease [48]. Although viscosity changes are not considered causes of these diseases, blood plasma viscosity could be used as a marker to indicate presence or severity of disease, response to therapy, or in characterizing the disease process.

Blood and blood plasma viscosity may become abnormal due to many pathologic conditions. While the viscosity of whole blood is primarily determined by hematocrit, changes in plasma viscosity have been observed in conjunction with various diseases, mostly associated with altered protein levels [27,49,65]. Examples include infections and infarction [27], hypertension [43] and diabetes [50]. Protein-induced hyperviscosity may lead to further complications [49], such as elevated risk of atherosclerosis [54]. Furthermore, one of the adverse effects of smoking is elevated plasma viscosity [15], which may contribute to the link between cigarette consumption and cardiovascular disease. Non-pathologic conditions may also influence blood and blood plasma viscosity. Examples include extended bedrest[16], pregnancy [30], and aging [60]. Viscosity changes in aging may also be attributed to indirect effects, such as age-related changes in habits (increased smoking, lack of exercise) [11]. In light of these observations, plasma viscosity has been proposed to be used as a diagnostic tool that allows early detection of diseases [27]. Blood viscosity becomes a crucial element in severe hemorrhage when hemodilution leads to dramatically lowered hematocrit and plasma viscosity. Blood viscosity should be monitored during transfusions and plasmapheresis [49].

Whole blood viscosity is determined by both fluid and cellular components

[38]. In large vessels that make up the central vasculature made up of arteries and veins (diameter >100μm), whole blood viscosity is proportional to the square of hematocrit of normal patients [64]. Blood viscosity is much less dependent on hematocrit in small diameter vessels such as capillaries with diameter close to the size of RBCs [64]. Plasma interacts with endothelial cells of vessel walls which regulate autocoid (prostacyclin, nitric oxide) release [62]. Prostacyclin and nitric oxide are potent vasodilators. Increased blood viscosity reduces peripheral vascular resistance and increases tissue perfusion [64]. Tsai and Intaglietta reported finding tissue perfusion is more dependent on blood viscosity than oxygen content [64]. With significant blood loss and reduced blood viscosity, inadequate viscosity correlates with decreased functional capillary density and decreased perfusion of capillary beds in peripheral tissues and vital organs such as the liver and kidneys [64].

These results indicate that in the event of significant blood loss, return blood viscosity as quickly as possible may limit damage to these vital organs. It has been shown that blood expansion with high-viscosity fluids enhances capillary perfusion and thus tissue oxygenation [63,64]. For many related purposes, including viscosity-related research, diagnosis of cardiovascular disease, or monitoring of the blood resuscitation process, a viscometer that is capable of fast serial measurement with low volumes is desirable . Mechanical viscometers fail to meet these demands. A new approach that has been recently introduced involves fluorescent viscosity-sensitive dyes, commonly referred to as molecular rotors.

7

1.4. Fluorescence

Fluorescence is the emission of light from a molecule in an excited energy state. Molecules may be excited from their lowest energy (ground) state to a higher energy state by absorption of a photon of appropriate energy. The molecule returns to its ground state through conversion of energy by vibrational/thermal relaxation with or without emission of light (fluorescence).

The exact position of an electron at any point in time cannot be known exactly but can be estimated according to Schroedinger's wave equation. This equation accounts for proton-electron electrostatic interactions, internuclear vibrations and rotational movement of atoms and molecules to determine the probability density of an electron's position about an atom's nucleus. This probability density is represented as "orbitals" and are complex 3-dimensional functions. These orbitals are distinct energy levels and an electron is prohibited from existing between ortbitals.

Each orbital may hold a maximum of 2 electrons and is assigned a principal quantum number (n) and angular momentum quantum number (l) according to its energy. Orbitals of the same principal quantum number (n=1,2,3...) are grouped into "shells" which can hold $2n^2$ electrons. Shells are further divided into subshells according to each electron pair's angular momentum quantum number (l=0,1,2,..n–1). Each subshell may hold 2l+1 electron pairs. For atoms in the lowest energy (ground) state, electrons must occupy the lowest energy orbitals possible.

Atoms bond together by sharing electrons. In general, stable bonds are

8

formed between atoms when outer or valence shells become filled. For example, hydrogen (^{1}H) in its ground state has only one electron (n=1, l=0) and is designated $1s^1$. A single hydrogen atom may form stable bonds with only one other atom, thus filling its valence electron shell ($1s^2$). Carbon (^{12}C) has 6 electrons: 2 in the first shell ($1s^2$), and 4 in the valence shell ($2s^2 2p^2$) in the ground state, leaving 4 spaces open. Thus, a carbon atom may form stable bonds with up to 4 other atoms.

When carbon forms bonds with 4 other atoms, a 2s electron is promoted to a p orbital and 4 equivalent sp^3 hybrid orbitals are formed. These bonds are called sigma bonds, and result from the sharing of electrons on the same plane. Carbon atoms may also form bonds with only 3 other atoms. In this case, three equivalent sp^2 orbitals are formed in the
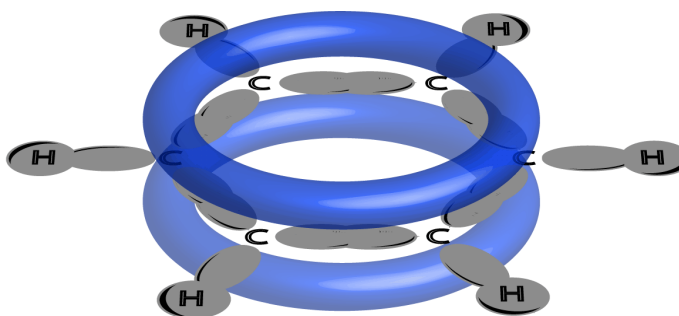
Figure 4: Benzene ring with σ bonds between individual carbons and hydrogens and delocalized π bond network. (Redrawn with permission from [5])

same plane and one p-orbital remains unchanged and perpendicular to the hybrid sp^2 orbitals. The sp^2 electrons are shared in sigma bonds while the electrons in the unchanged p-orbitals of adjacent molecules then associate to form π bonds, represented as double bonds between carbons or other capable atoms such as oxygen. In aromatic molecules (organic molecules that contain benzene rings), the π bonds

become shared or delocalized throughout the π bonding network (Fig 4) [5].

1.4.1. Absorption

A molecule may absorb energy that alters its electronic configuration. Ionizing radiation such as Xrays and high energy ultraviolet (UV) light may interact with inner shell electrons and cause the expulsion of electrons, creating highly reactive radicals. This type of radiation may damage genetic material in cells, causing tissue destruction which may lead to cancer. Lower energy radiation such as low energy UV, visible light and infrared light only affects outermost electrons. Molecular energy transitions correspond to electron movements between orbitals.

Light is composed of photons that have both particle and wave properties. Photons are discrete packets of energy. A photon's energy is dependent on its wavelength:

$$E = \frac{hc}{\lambda} \tag{5}$$

where h is Planck's constant (h=6.625×10^{-34} Js), c is the speed of light in a vacuum, and λ is wavelength. Thus a blue photon with a 400 nm wavelength contains more energy than a red photon with a wavelength of 700 nm.

Light absorption occurs when the resonance frequency of the dipole moment exactly matches the frequency of the incident photon. Transient dipoles

may be induced in molecules without permanent dipoles by placing them in a magnetic field. Dipole oscillation occurs with frequency related to the size of the transition dipole moment. The intensity of an absorption band is directly related to the transition dipole moment of the electron transition. The energy required for the transition of a sigma electron to a higher orbital (sigma*) requires a photon with wavelength less than 200 nm. A $\pi \rightarrow \pi^*$ transition for aromatic molecules may occur with absorption of a photon in the near UV and visible light range (300 nm - 700 nm). Transition from the excited state to the ground state ($S_1 \rightarrow S_0$) occurs by nuclear vibration and rotation, internal conversion, and/or photon emission.

1.4.2. Emission

Fluorescence is the emission of a photon by a molecule after absorption of a photon of higher energy. There are many different molecules that have fluorescent characteristics. Most fluorescent molecules have aromatic rings that allow delocalization of charge among multiple π orbitals.

The process of energy
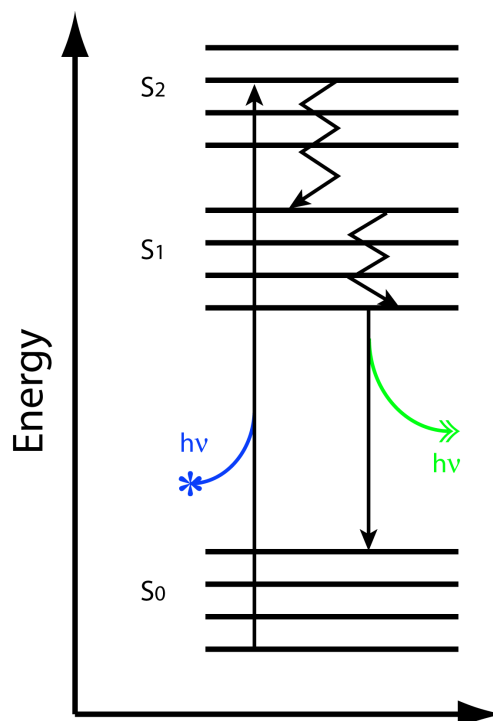
Figure 5: Jablonski energy diagram for process in fluorescence. Fluorescent molecules absorb a photon (hv) and are excited to a higher energy state (S_1, S_2), then return to the ground state (S_0) by internal conversion or photon emission. Emission occurs from the lowest excited singlet state.

11

absorption and emission by a fluorescent molecule is represented by the

Jablonski energy diagram in Fig 5. Absorption of a photon excites the molecule

from its ground state S_0, to a higher energy state. From the lowest excited singlet

state S_1, the molecule may undergo one of three processes: internal conversion,

fluorescence, or intersystem crossing. Internal conversion is the release of

energy in thermal processes and does not lead to photon emission.

Fluorescence is the release of energy in the form of a photon of lower energy

(longer wavelength) than the photon absorbed. Intersystem crossing is the

transition of the molecule from S_1 to a lower energy triplet state, T_1 , the source of

phosphorescence. The quantum yield of a dye is related to these three

phenomena by:

$$\Phi = \frac{k_F}{k_F + k_{nr}} \tag{6}$$

where k_{nr} represents the rate constant for all non-radiative $S_1 \rightarrow S_0$ transitions

which include internal conversion, intersystem crossing and quenching, and k_F is

the fluorescence rate constant. At room temperature and in the absence of

quenching, intersystem crossing is negligible and internal conversion is the main

determinant of k_{nr}.

The average time the molecule spends in the excited state prior to return

to the ground state is called fluorescence lifetime, τ:

$$\tau = \frac{1}{k_F + k_{nr}} \qquad (7)$$

Typically, fluorescence lifetimes are typically several nanoseconds.

1.4.3. Spectra

A photon emitted via fluorescence after single-photon excitation is of lower energy (longer wavelength) than the exciting photon. The wavelength of light emitted as a photon "jumps" from a higher energy orbital to a lower energy orbital is:

$$\lambda = hc / \Delta E \qquad (8)$$

In general, the larger the dipole moment created by the electron sharing, the lower the energy of emission because of the increased stability of the excited state.

The Frank-Condon principle states all electronic transitions occur without change in nuclear position. A molecule may be excited to a higher energy state, but emission is most likely from the lowest excited singlet state (S_1). All else being equal, the observed emission spectrum of a fluorophore will be the same regardless of excitation wavelength, only intensity will be different [39].

The emission depends on the difference between the potential energy of the excited molecule and the ground state. Fluorescence emission is most likely to occur from the lowest excited singlet state and is generally represented by the

13

peak of the emission spectra. Simple absorption and emission spectra of a fluorophore are usually spread in a Gaussian distribution and obey the mirror image rule. More complex spectra result from the presence of multiple ground or excited state configurations. The spread is explained by vibrational energy states as represented by Fig. 5. Fluorescence spectra represent the detection of emission from many fluorophores at slightly different vibrational energy states.

1.4.4. Quenching

Any process that decreases fluorescence intensity of a sample is called quenching [39]. In this discussion, only factors that affect fluorescence of a molecule after absorption of a photon will be considered quenching. These processes include excited-state reactions, molecular rearrangements, energy transfer and collisional or dynamic quenching. Excited-state reactions include general and specific effects of solvents on fluorophore emission. Some fluorophores may undergo conformational changes in the excited state that affect emission. Dynamic quenching occurs when a molecule collides with an excited-state fluorophore within its fluorescence lifetime.

Dynamic quenching is dependent on the concentration and temperature dependent diffusibility of the quencher. Dynamic quenching is described by the Stern-Volmer equation (Eq. 9):

$$\frac{F_0}{F} = 1 + k_q \tau_0 [Q] \qquad \textbf{(9)}$$

where Q is the quencher concentration, τ_0 is the fluorescence lifetime of the fluorophore, and k_q is the temperature-dependent quenching constant. The quenching mechanism is not completely understood. Collision of the fluorophore and quencher lowers the energy of the fluorophore so that no emission occurs. Oxygen is a quencher of all known fluorophores.

An eximer is the result of interaction of an excited-state fluorophore with an unexcited molecule of the same species. Eximers have distinct photophysical properties including fluorescence. Exiplexes are similar to eximers except they result from interaction of an excited -state fluorophore with unexcited aromatic or other molecule. Both eximers and exiplexes exhibit unique emission spectra or are not fluorescent.

General solvent interactions may also affect fluorescence. Fluorophore emission spectra depends on the energy of the excited-state. A process that stabilizes the excited state prior to emission results in lower energy fluorescence. This shift to lower energy, longer wavelength emission is called a bathochromic or red shift.

For most fluorophores in polar solvents such as water and ethanol, emission wavelength is red-shifted compared to emission wavelength in nonpolar solvents. Polar solvent molecules arrange around dissolved molecules to minimize the interaction energy. This arrangement is called the "solvent sheath". A fluorophore's excited state dipole moment is larger than the ground state dipole moment. The solvent molecules must reorient to minimize total energy. Relaxation of the solvent sheath of small MW solvents occurs within the

15

fluorescence lifetime of most fluorophores. This relaxation stabilizes the excited state of the fluorophore and reduces the energy of emission, shifting it to a longer wavelength. Photon absorption occurs instantaneously (10^{-15} s) while emission from the excited state depends on the fluorescence lifetime of the fluorophore. The change in emission spectra is greater for more polar fluorophores and in highly polar solvents. Solvent sheath relaxation is slower at low temperature.

Solvent interactions that are specific to solvent-dye systems include pH, hydrogen bonding and charge transfer. Change in a molecule's structure such as ionization or protonation will affect its photophysical properties. These are more complex than general solvent effects and may confuse results if not recognized.

Fluorescence is also generally sensitive to temperature. Solvent relaxation is slower at low temperatures. Molecular vibration is also less at low temperatures which increases the likelihood of fluorescence, quantum yield.

1.4.5. Instrumentation

Fluorescence is measured via fluorospectrophotometer. The excitation light is passed through the sample similar to a simple spectrophotometer, but the emitted light is measured perpendicular to the excitation path. Fluorescence intensity is several orders of magnitude less than that required for excitation and depends on the concentration and quantum yield of dissolved fluorophore. In most commercial spectrofluorophotometers the excitation light is provided by an arc lamp, which has a broad spectrum. The light for excitation is filtered by a monochromator before light hits the sample. Monochromators are gratings that

diffract light. Another monochromator is used to separate scattered excitation light from fluorescence emission. Other methods of illumination include monochromatic lasers and high intensity light emitting diodes (LED), but they do not have much spectral range. Wavelength-limiting filters such as dichroic mirrors can also be used to separate excitation and emission paths. Filters also limit the flexibility of systems.

A fluorometer measures the signal intensity from a sample, which is the average number of photons detected integrated over the collection time. This intensity is dependent on many factors other than the fluorescence quantum yield of the dye. Measured intensity is related to the intensity of excitation, sample optical properties, scattering and light loss in the instrument and sensitivity of the electronic sensor. Sample optical properties include the dye concentration and any other absorbing or scattering components.

Absorption of fluorescence energy by fluorophores of the same species as the emitter is called the inner filter effect and is considered significant in samples with optical density greater than 0.1 [39]. For many situations, the sample of interest has components that absorb excitation and/or fluorescence energy and may fluoresce as well, which is common in biological samples. In these samples, background absorption and emission leads to a noisy signal and makes quantitative measurements difficult. For example, the fluorescent probe, calcium green, has much greater quantum yield in the presence of calcium, which can be detected as higher intensity. For quantitative calcium measurement, the concentration of calcium green must be known with great precision, which is

difficult in biological samples.

The most common configuration for detection of fluorescence in fluid sample is right-angle detection (Fig. 6). It is possible to correlate fluorescence intensity with fluorophore concentration by measuring the absorption of excitation light simultaneously with fluorescence. Such methods and devices have been proposed [8,57,31,51] but a commercial device is not available at this time.
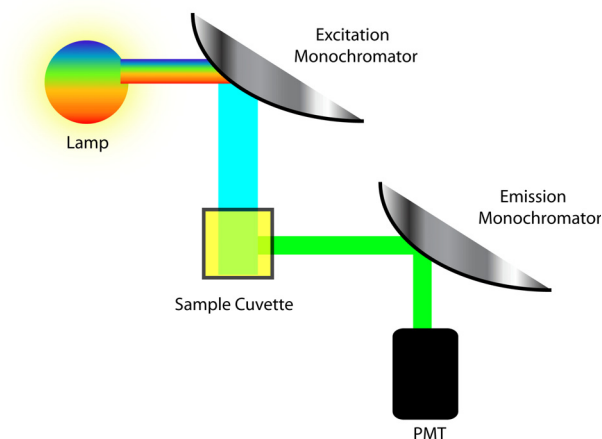
Figure 6: Simplified schematic for a right-angle fluorometer using a full-spectrum arc lamp as the excitation source and photomultiplier tube (PMT) for fluorescence detection. Fluorescence is measured at perpendicular to the excitation beam. Excitation and emission light is selected by adjustable monochromators.

1.5. Fluorescence Sensing

Since its discovery more than a century ago, fluorescence has been developed into a broadly useful sensing technique for biological research. Fluorescence sensing has replaced radiographic techniques in many procedures because, unlike radioactive materials, fluorescence techniques do not produce tissue-damaging radiation. Fluorescence may use ultraviolet, visible or infrared light for excitation.

Living systems contain naturally occurring (intrinsic) fluorophores. The

intrinsic fluorescence of proteins and other factors in biological tissues has been used for studying disease pathology on the microscopic and macroscopic scale. The aromatic amino acids tyrosine, tryptophan and phenylalanine, components of most proteins, are fluorescent. Cofactors such as NADH and flavins such as FAD are also fluorescent. Fluorescence from intrinsic fluorophores in tissues is termed autofluorescence. The optical properties including autofluorescence of healthy tissues tends to be measurably different than that of cancerous tissue.

Synthetic fluorescent probes, also called extrinsic fluorophores, have been developed that are highly sensitive to system chemical and physical properties such as pH, temperature, chemical concentration, and others. These include fluorescent analogs of non-fluorescent biomolecules, such as DNA bases adenine and guanine, and cell process cofactors. Extrinsic fluorophores have been developed for sensing specific ion concentration, oxygen concentration and pH, temperature, cell membrane potential, and solvent polarity. Many fluorophores selectively localize to certain regions of the cell and are useful for imaging the cell membrane, nucleus, mitochondria and other organelles. Proteins may be labeled with fluorophores for cell process tracking and for immunofluorescent assays. Fluorescence from extrinsic fluorophores must be separated from tissue autofluorescence. Probes used in tissues generally have much greater signal strength than intrinsic fluorophores, or emit at different wavelengths.

Lipid soluble probes localize in the cell membrane. Probes adhere specifically to DNA can be used to watch the progression of mitosis and meiosis.

Other probes are specific to the cytoskeleton and allow visualization of actin filaments during cell locomotion.

Fluorescent probes are used to label proteins such as antibodies in biosensors. Immunofluorescent assays use fluorescently labeled antibodies to detect the presence of bacteria, virus, or other disease antigens.

The specific properties of some fluorescent probes allow sensing in single cells and organelles within cells in vivo. Probes are used to determine calcium concentration changes during heart muscle cell depolarization that causes the heart to beat. Probes can also detect the relative oxygen concentration in cells.

1.6. Molecular Rotors

Lippert and others published a description of anomalous dual fluorescence from 4,4'-dimethylaminobenzonitrile (DMABN) [59]. Initial explanations of the mechanism of dual fluorescence included solvent sheath reorientation [21], eximer formation [21] and proton transfer [21]. These hypotheses were refuted by Grabowski and others in favor of the twisted intramolecular charge transfer (TICT) model, based on the parallel polarization of both emission bands [21], evidence of concentration independence of dual fluorescence ratios [21], and existence of dual fluorescence in aprotic solvents [21].

Further studies by Grabowski and others led to the resolution of the TICT as the mechanism of dual fluorescence of DMABN and other molecules and their free-volume dependent fluorescence yields. Grabowski and others investigated the mechanism of TICT by comparing similar molecules with structures

20

systematically varied to inhibit molecular conformation changes at points of possible rotation [21].

Grabowski hypothesized that in the excited state, delocalized π, π* energy sharing may be disrupted by intramolecular rotation, causing localization of the charge on the donor (+) and acceptor (-) respectively. The energy of the lowest excited singlet state of the twisted molecule is lower than that of the planar form while the twisted ground state is higher than that of the planar ground state (Fig. 8). This situation results in much easier internal conversion of energy lower fluorescence probability from the twisted state.

An energy barrier exists between the planar and twisted isomers which is not significant at normal temperatures, but becomes significant in high viscosity solvents and at very low temperatures. In a volume-restricted environment, the energy barrier is elevated, decreasing internal rotation and increasing fluorescence yield. This energy barrier is responsible for the viscosity sensitivity of molecular rotors. The twisted molecular form is not energetically favored in the ground state. Therefore, molecular rotor absorption is independent of viscosity and can be used to determine concentration according to Beer's law.

Loutfy and Law investigated three p-N,N-dialkylaminobenzylidene-malononitriles, including 9-(dicyanovinyl)-julolidine (DCVJ), molecular rotors with two cyanine groups, which form a better acceptor than the single cyanine of

DMABN [47]. These molecular rotors have TICT characteristics due to rotation

points at the N-R$_2$ and/or carbocyanine groups. They found that the rigidity of the

N-R$_2$ group corresponds with higher fluorescence quantum yield in all solvents

tested due to the "free rotor effect" of the non-rigid N-Me$_2$

of Dye 1 (Fig 7). They calculated the activation energies of

each from the temperature sensitivity of their quantum

yield. They compared the fluorescence lifetimes of the

three dyes and found that DCVJ fluorescence lifetime is

much greater than that of Dye 1. The TICT-forming

molecular rotors exhibited viscosity sensitivity without

polarity sensitivity in alcoholic solvents with viscosity

greater than 2 mPa s [45]. They also observed

Figure 7: Dye 1 in [47].

fluorescence quantum yield of the three dyes approached
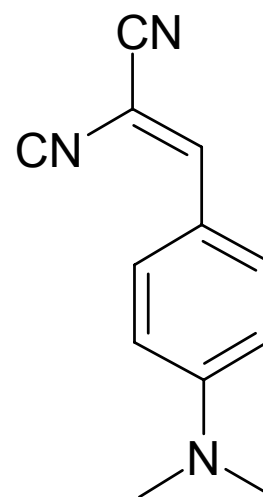
unity in 2-MeTHF glass matrix at 77K. Intersystem crossing was not observed for

any of the dyes. Viscosity sensitivity of DCVJ is attributed to rotation about the

C=C double bond similar to stilbenes and carbocyanines previously studied [41].

Förster and Hoffman [18], described the mathematical relationship between

solvent viscosity (η) and fluorescence quantum yield (Φ) as:

$$\log \Phi = x \cdot \log \eta + C \qquad \textbf{(10)}$$

where x is a dye dependent factor, and C is a temperature-dependent constant

[24]. Law derived the Förster-Hoffman equation from Doolittle's free volume

equation and the theory of free volume quantum yield dependence of molecular
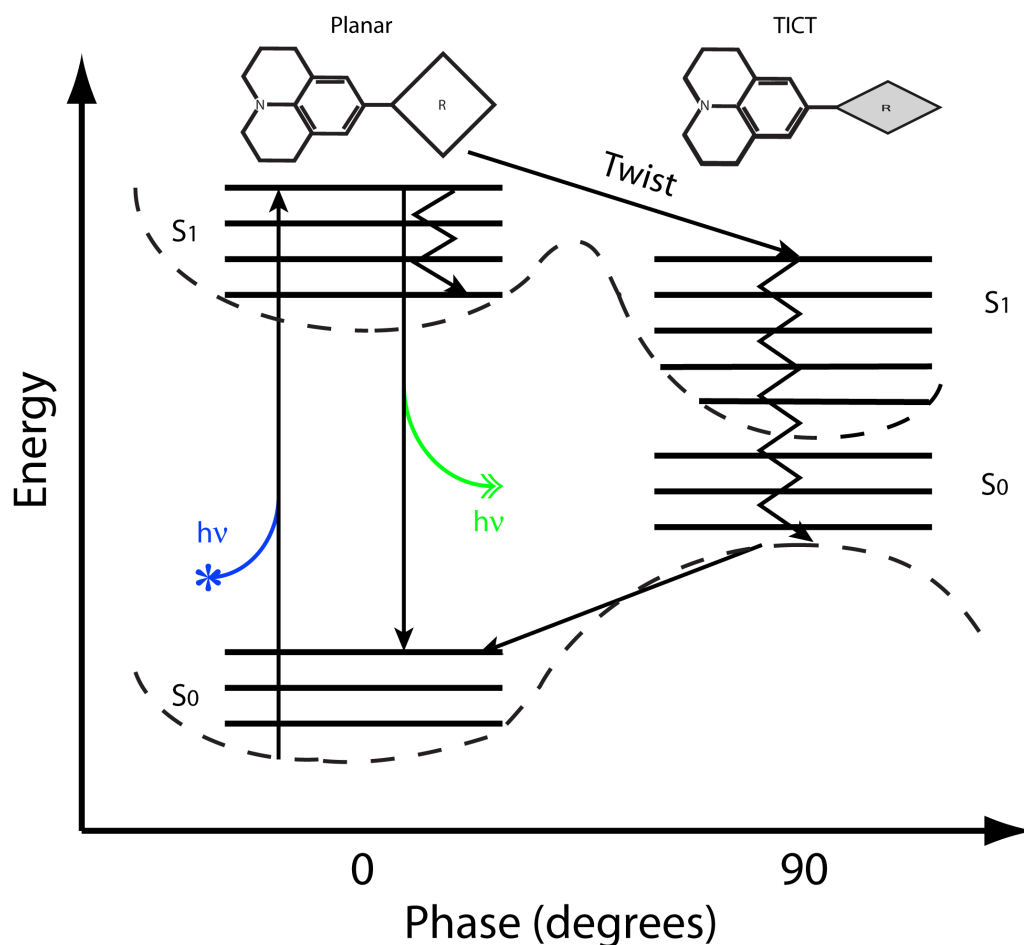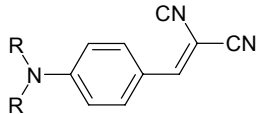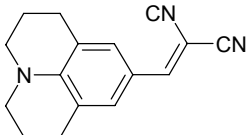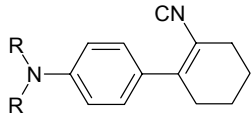
Figure 8: Energy diagram for molecular rotor fluorescence and internal conversion by rotation. Dashed line represents idealized potential energy for planar and twisted ground (S_0) and excited (S_1) states.

rotors [41].

In another article, Law discussed the same dyes in relation to their viscosity sensitivity in alcoholic solvents [41]. Law observed that the rotors were insensitive to viscosities lower than 2 mPa s. For long-chain alcohol solvents, molecular rotor quantum yield did not correlate with viscosity, but decreased with chain length greater than carbons. Law's hypothesis was that entanglement of the chains led to increased free volume as sensed by the rotors despite

Table 1: Three of the molecular rotors investigated in [1] with quantum yields relative to quininie bisulphate as fluorescence standard. Quantum yield correlates with rotation points in molecular rotor structure.

Molecular Rotor			
Quantum Yield	900	3000	10000

increased overall solvent viscosity.

Abdel-Mottaleb and others compared photochemical properties of several molecular rotors with respect to channels of internal conversion [1]. They found fluorescence quantum yield increased with molecular rigidity. Rotors with more deactivation channels had lower quantum yield.

In fluoroscopy the emission intensity I is determined, which is proportional to the quantum yield, but also depends on excitation light intensity, cell geometry, dye concentration and other factors. Equation 10 can be rearranged to yield viscosity from intensity [24]:

$$\eta = (\kappa \cdot I)^{\nu} \tag{11}$$

where emission intensity I replaces quantum yield, $\kappa \propto 10$-C and v= 1/x. The constant κ represents instrument factors in addition to those factors represented by C in Eq. 10. These constants need to be determined empirically by calibration with known viscosities.

CHAPTER 2.

A MOLECULAR ROTOR AS VISCOSITY SENSOR IN AQUEOUS COLLOID SOLUTIONS

2.1. Introduction

Colloidal starch solutions, such as aquesous solutions of dextrans and hydroxyethyl starches (HES) are used for expansion of plasma volume [26,10,13,34,40]. These are solutions of large molecular weight (MW), variably branched carbohydrate polymers that help maintain intravascular oncotic pressure [61]. Perfusion of small capillary beds and tissue oxygenation become significantly reduced with low blood viscosity, as in the event of severe blood loss. Administration of plasma expanders increases blood viscosity and improves tissue oxygenation [63,64].

Dextrans are highly branched polysaccharides of varying length, extracted from *Leuconostoc mesenteroides* bacterial culture [29]. Most branches in dextran originate from the primary polysaccharide backbone. The dextran molecules have a high degree of dextrorotation, forming coils which coalesce to be roughly spherical molecules in aqueous solutions [61].

Hydroxyethyl starches (e.g. hetastarch and pentastarch) are made from plant-derived amylopectin and vary by molecular weight and degree of substitution of hydroxyl groups by hydroxyethyl groups. Branching is more complex in HES than in dextran, with branches originating from other branches in a tree-like fashion. Amylopectin forms spheres of Gaussian density consisting of

tight, ordered helices in solution, with the helices having hydrophobic cores [19]. Hydroxyethyl starches are not metabolized as quickly as dextrans. HES can maintain intravascular oncotic pressure for longer times and thus needs to be administered less frequently [6].

This study evaluated the viscosity sensitivity of CCVJ, a hydrophilic molecular rotor, in aqueous plasma expander solutions of varying viscosities.

2.2. Materials and Methods

Reagents purchased as follows: CCVJ from Helix Research (Springfield, OR), fluoroscopy grade DMSO from Sigma (St. Louis, MO), Pentaspan (10% pentastarch in 0.9% NaCl, average MW 260 000) from Dupont (Wilmington, DE), Hetastarch (6% in 0.9% NaCl, avg. MW 670 000) from Abbott Laboratories (North Chicago, IL). Dextran (77 800 and 249 000 average MW) from Sigma (St. Louis, MO), was used to prepare 7% solutions of each, and of a 2 parts 77.8 kDA to 1 part 249 kDa mixture in 0.9% NaCl. Fluorescence and absorbance spectroscopy were performed in methylacrylate microcuvettes (Fisher Scientific, Pittsburgh, PA,) using Spex Fluoromax-3 (Jobin-Yvon, Stanmore, North London, UK,) and a Beckman DU 520 spectrophotometer, (Beckman Coulter, Fullerton, CA,) respectively.

Crystalline CCVJ was dissolved in DMSO to make a 20 mM stock solution. Ten μL of stock CCVJ was dissolved in 5ml of 0.9% NaCl in water prior to making samples to reduce mixing errors. Sample viscosity was modulated between 1.0 and 5.0 mPa·s by varying concentration of starch solutions within

the saline solution. Total sample volume was made to be 1.0 mL, with 50 μL of prestained solution in each sample. To account for variations in dye concentration due to solubility, absorbance at 440 nm was measured in each sample for normalization. Individual data sets were combined by normalizing the y-intercepts of plots of log intensity versus log viscosity to correct for concentration differences. Emission scans were then performed for wavelengths of 460-510 nm, with excitation wavelength of 440 nm, 2nm slits, and 0.1 s integration time.

Physical viscosity measurements were made with Brookfield DV-III+ (Middleboro, MA) cone-plate viscometer with CPE-40 spindle. Samples for viscosity measurements were 0.5 ml and measured at discrete shear rates: 150, 300, 450, 600, and 750 s^{-1}, (20, 40, 60, 80, and 100 rpm). The plate unit was kept at a constant temperature of 24˚C with water circulating from a temperature-controlled waterbath. Comparison to intensity was performed with viscosity values taken at 60 rpm (450 s^{-1}). This shear rate was chosen to remain within instrument accuracy limits, and to reduce any apparent non-Newtonian effects on results: while noticeable instrument fluctuations as well as apparent shear-thinning effects existed at shear rates of 300 s^{-1} and below, no visible influence of shear rate on measured viscosity existed at 450 s^{-1} and above.

Statistical analysis was performed using one-way ANOVA with a post test for linear trend between groups (Graphpad Prism 4.0, Graphpad Inc, San Diego), where a group comprised all intensity measurements taken with the same starch type at the same starch concentration. Determination of the relationship between

viscosity and intensity was performed through linear regression of the

logarithmized data, where the slope was taken as the value *x* in Equation 16.

For hetastarch and pentastarch, only points above 1.5 mPa s were used.

2.3. Results

2.3.1. General observations

The molar extinction coefficient ϵ for CCVJ in water was determined to be

25404 $M^{-1}cm^{-1}$ at 440 nm, Unlike emission intensity, the absorbance *A* is

independent of solvent viscosity. CCVJ concentrations ranged from 1.2 μM to 3.9

μM between experiments. As shown in Fig. 9, CCVJ emission intensity increases

strongly with increased fluid viscosity, and absorbance increases with CCVJ

concentration. Only a minor increase of absorbance can be seen with increased

viscosity which is caused by the higher starch concentration and is also observed

in starch solutions without CCVJ.
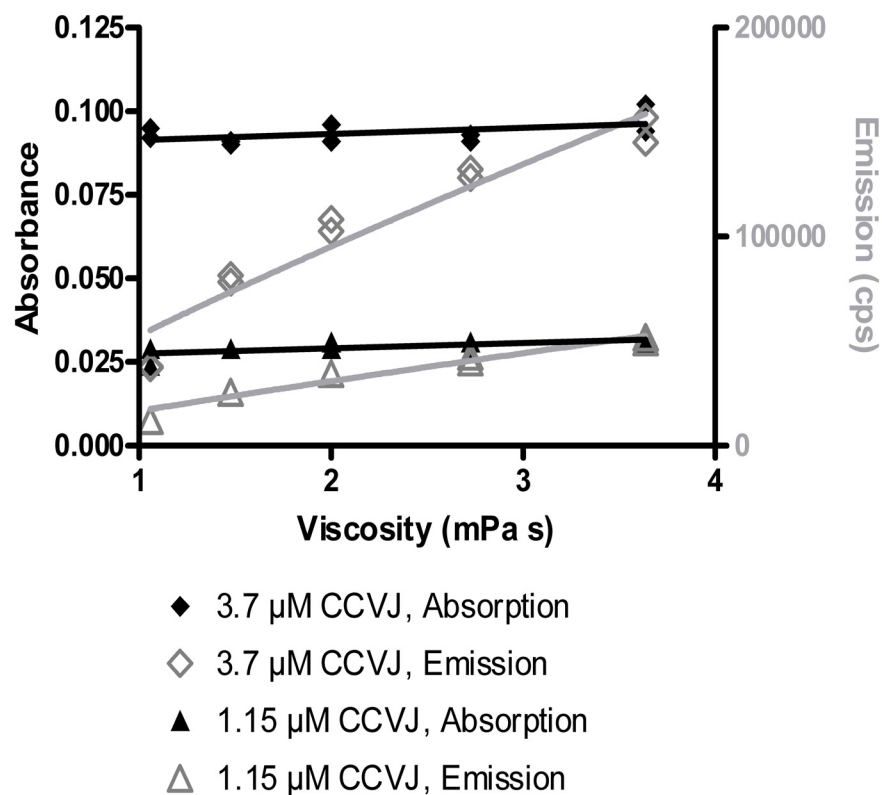
Figure 9: Comparison of CCVJ absorbance and emission at different CCVJ concentrations and viscosities modulated by hetastarch content. While emission intensity increases with both CCVJ concentration and viscosity, absorbance increases strongly with concentration only. Lines are for comparison only and are not meant to imply linear relationship is best fit.

Therefore, *A* is a function of the dye concentration *c* and cuvette length *l* (10 mm) according to Beer's law (Equation 12):

$$A = \varepsilon \cdot l \cdot c \qquad \textbf{(12)}$$

Using the viscosity-independent absorbance, it was possible to adjust emission

intensity to eliminate differences in CCVJ concentration in all cases using

Equation 13:

$$I_{eff} = I \cdot \frac{A_{nom}}{A} \tag{13}$$

where I is the measured intensity, A is the corresponding absorption, A_{nom} is the

nominal absorption calculated from concentration and molar extinction

coefficient, and I_{eff} is the effective (corrected) intensity. In the following sections,

I_{eff} is used exclusively.

2.3.2. Comparison of dextran solution viscosity to CCVJ fluorescence.

Figure 10 shows the experimental results of CCVJ fluorescence in dextran

solutions of varying concentration of different MW. The logarithmic relationship

of intensity to viscosity fits the Förster-Hoffman model, Equation 10. The slopes

of the resulting lines increased with decreasing MW, and are close to the

theoretical value of 2/3. Figure 11 shows the emission spectra for CCVJ in

dextran solutions of varying viscosity. The intensity peak for CCVJ in dextran is

496nm in all cases. For all MW dextran solutions, mean CCVJ fluorescence

intensities showed positive correlation with solution viscosity and were

significantly different between each viscosity group (ANOVA, $p < 0.0001$) with a

significant linear trend ($p < 0.0001$).
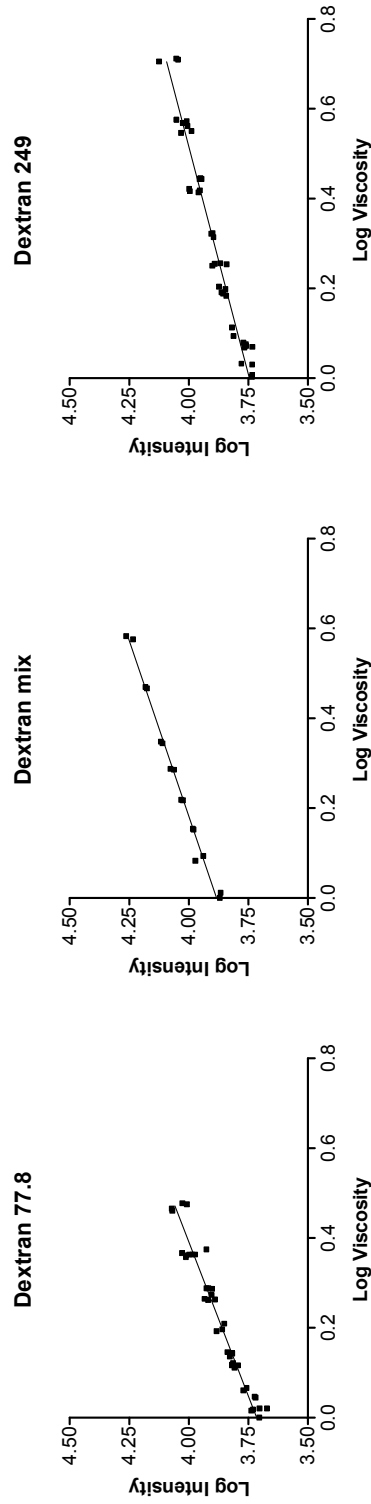
Figure 10: CCVJ fluorescence intensity versus fluid viscosity in solutions of dextran with relatively small molecular size (77.8 kDa), large molecular size (249 kDa) and a mixture: two parts dextran 249 to one part dextran 77.8. Viscosity was measured in a cone-and-plate viscometer at a shear rate of 450 s^{-1}. The graphs for dextran 77.8 and 249 are combinations of four sample sets each (N=15, 10, 10, and 6). In order to combine them, the y-intercept (the constant C in Equation 11) was normalized was normalized with respect to concentration as determined spectroscopically, thus eliminating concentration fluctuations. A good fit of a straight line in the double-logarithmic scale indicates a power-law relationship between intensity and viscosity over the entire viscosity range. The slopes are 0.72 (r^2=0.95; 77.8 kDa), 0.49 (r^2=0.95; 249 kDa) and 0.64 (r^2=0.99; mix), respectively.

31
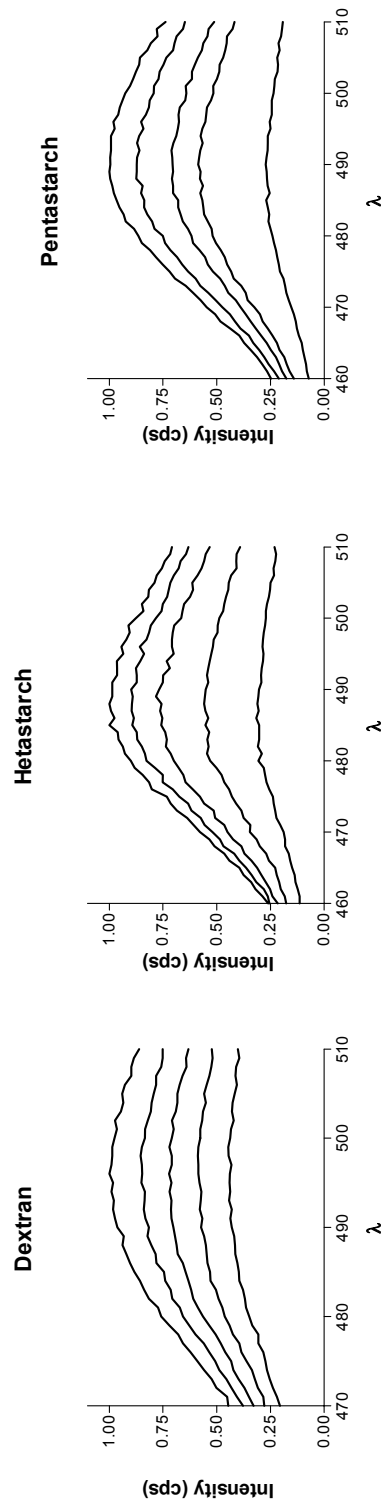
Figure 11: Typical CCVJ emission spectra in dextran, hetastarch and pentastarch solutions. CCVJ fluorescence emission peak occurred at 490 nm in all dextran solutions and 496 in all hetastarch and pentastarch solutions.

2.3.3. Hydroxyethyl Starch

Figure 12 shows the results of viscosity and fluorescence measurements with CCVJ in hetastarch and pentastarch solutions respectively. The relationship of CCVJ fluorescence to solution viscosity appears multiexponential, with two different slopes at viscosities above and below 1.5 mPa·s. For viscosities greater than 1.5 mPa·s the data closely follows a straight line (Fig. 13). Only those data points have been used to compute a slope (value of x in Equation 10). Peak CCVJ fluorescence intensity occurred at 490 nm, independent of starch concentration (Fig. 11). Intensity of CCVJ fluorescence in HES solutions was higher than in dextran solutions by a factor of 5. For both pentastarch and hetastarch, mean intensities were significantly different between each viscosity group (ANOVA, $p<0.0001$) with a significant linear trend ($p<0.0001$).
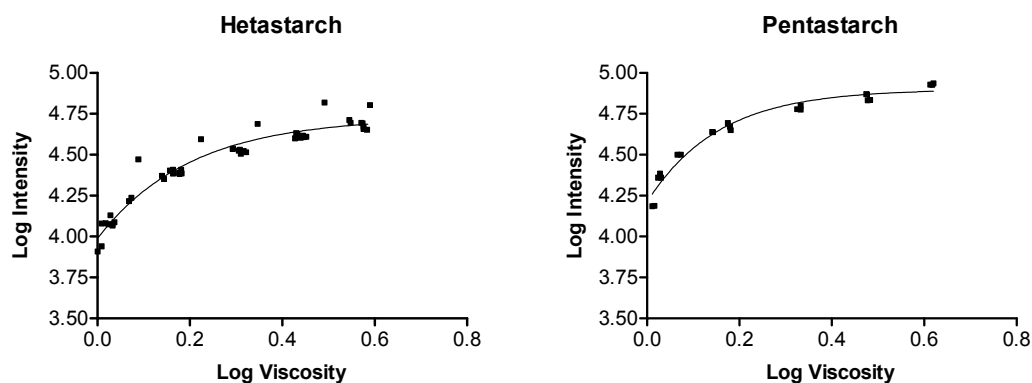
Figure 12: CCVJ fluorescence intensity vs. fluid viscosity in solutions of hetastarch and pentastarch. Viscosity was measured in a cone-and-plate viscometer at a shear rate of 450 s^{-1}. As opposed to dextran, the intensity-viscosity-relationship is biexponential with a higher slope in the low-viscosity range. A very good fit of a straight line can be achieved in the viscosity range from 1.5 mPa s to 6.0 mPa s which yields the exponents (slopes) 0.73 (r^2=0.96; hetastarch) and 0.59 (r^2=0.97; pentastarch).
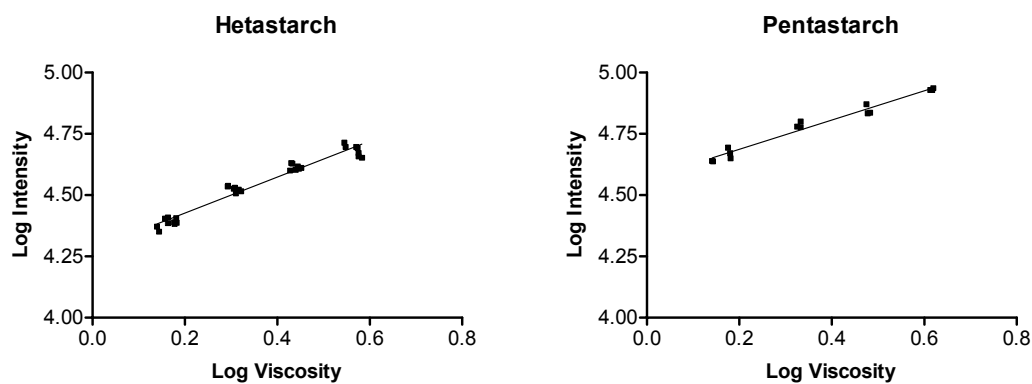
Figure 13: Log intensity versus log solution viscosity for hetastarch and pentastarch solutions with viscosity greater than 1.5.

The computed slope of the double-logarithmic fit is given in Table 2 for all solutions. Very high correlation coefficients of intensity with viscosity were found in all cases. From these data points, the constants κ and v were computed to obtain the calibration curve, Equation 11. Those values are listed in Table 3. A first estimate of the method's precision is possible by computing the deviation of the individual points from the calibration curve (residuals). Given the calibration curve, Equation 11, the relative deviation R_i of the fluorescence-based viscosity from the mechanically determined viscosity η_i was computed using Equation 14:

$$R_i = \frac{\eta_i - (\kappa \cdot I_i)^v}{\eta_i} \cdot 100\% \qquad \textbf{(14)}$$

where i denotes the i-th data point, I_i denotes the corresponding peak emission intensity, and κ and v are the calibration constants obtained by regression. R_i was in the range -5.5% to +5.1% with an average over all experiments of 2.2%.

Table 2: Comparison of slope of log-log plot and correlation of data points for CCVJ intensity vs. viscosity of starch solutions studied. Slope corresponds to factor "x" in Eq. 1. The number of samples indicates the number of independent experiments performed under the same conditions.

Starch	Dextran 77.8	Dextran Mix	Dextran 249	Hetastarch	Pentastarch
Slope x	0.71	0.63	0.49	0.73	0.57
Number of samples	40	15	40	30	15
Correlation coefficient	0.97	0.98	0.99	0.98	0.94

Table 3: Comparison of $\eta = (\kappa \cdot I)^v$ variable values for starch solutions at given CCVJ concentrations used to calculate viscosity from measured intensity.

Starch Solution	[CCVJ] uM	κ	v
Dextran 77.8 kDa	1.14	0.000186	1.41
Dextran Mix	2.17	0.000127	1.59
Dextran 249 kDa	1.18	0.000174	2.04
Hetastarch	1.15	0.0000259	1.37
Pentastarch	1.37	0.0000524	1.77

2.4. Discussion

This study corroborates earlier results [24] that fluorescence emission of molecular rotors closely follows a power-law relationship with the solvent's viscosity (Eq. 10) in starch solutions where the viscosity-determining molecules are by orders of magnitude larger than the sensor molecule, CCVJ.

These results support those of Loutfy and Arnold [46] who showed that molecular rotation becomes increasingly restricted as viscosity increases and imposes steric hindrance on the rotors. It was demonstrated that with a similar molecular rotor in a glass at low temperature, internal conversion through molecular rotation decreases as free volume approaches zero, and quantum yield approaches unity [47]. Loutfy and Arnold demonstrated that in medium to high viscosity solvents, carbocyanine dyes adhere to this derived free volume model rather than the Debye-Stokes-Einstein hydrodynamic model which relies only on molecular size [46]. This observation could explain the deviation from the power-law relationship seen in Fig. 12 at low viscosities. While CCVJ emission follows the Förster-Hoffmann-relationship at viscosities above 1.5 mPa s, the steeper slope at low viscosities corresponds to the Debye-Stokes-Einstein hydrodynamic model.

The observed increase of emission intensity with solvent viscosity can be seen consistently in a large range of molecular rotor concentrations. While 25 µM were used in blood plasma-colloid mixtures [24], limited solubility of CCVJ in protein-free aqueous systems restricted the concentration to 5 µM and below. The fluorescence intensity of different concentrations of CCVJ can be normalized

between similar viscosity solutions using Eq. ? for at least a 3-fold range of concentrations.

Concentration is a prime determinant of the constant κ in Equation 11. If this is accounted for, optimum rotor concentration is found as a balance between poor emission signal at low concentrations and excitation light absorption (inner-filter effect) at high concentrations. The fluorometer used in this study was able to reliably pick up the emission signal at 5 μM; a further reduction seems possible. Above 25 μM, a significant inner-filter effect can be observed, and further increasing the concentration is not advisable.

CCVJ fluorescence intensity in dextran solutions with smaller average MW exhibit larger slope than solutions with larger MW. A mixture of these solutions produced an intermediate slope (Fig. 10). We hypothesize that this phenomenon is due to the spherical nature of dextrans in aqueous solutions. Intramolecular rotation of CCVJ would be more restricted in a solution of smaller spheres than larger with the same viscosity, because higher molecule density is required to achieve the same viscosity. Hence, the probability of CCVJ-dextran interaction is higher with smaller MW dextrans.

Hydroxyethyl starch is derived from amylopectin, which is thought to form tight helices in solution. The interior of the amylopectin coil is hydrophobic, and can accommodate small hydrophobic molecules [19]. CCVJ is more hydrophilic than those rotors previously studied [47,46,41] due to its carboxylic acid moiety, but is still soluble in solvents with low polarity due to its julolidine base. In dilute solutions of HES, it is conceivable that the starch molecules have relatively little

to no interaction with each other. In these solutions, quantum yield of free CCVJ should be near that in water. Even at the lowest concentration HES solution, intensity is much higher than in water, indicating that CCVJ must be associating with the starch molecules, likely within the hydrophobic helical cores. The absence of a blue-shift in the spectral data suggests that the association is non-covalent, and significant aqueous contact is still present. In experiments using a molecular rotor in polymerization reactions, quantum yield varied inversely with polymer length, which was attributed to increased free space within the polymer hydrocarbon chains, until molecular size caused restriction of intermolecular free volume [45]. As the HES concentration increased, there is greater starch-starch interaction, restricting the branch flexibility. This reduction of helix flexibility is seen by CCVJ as a reduction in rotational free space giving increased quantum yield with increasing starch concentration and therefore viscosity. This constitutes an alternative explanation for the effect seen in Figure 12 which shows a deviation from the power-law relationship between intensity and viscosity at viscosities less than 1.5 mPa·s.

The choice of a suitable molecular rotor depends on the solution to be measured. In solutions containing albumin and other proteins that can carry hydrophobic substances, as well as solvents such as methanol, ethylene glycol or glycerol, water-insoluble rotors can be used with the same efficiency as CCVJ [24] . In purely aqueous systems such as the colloid solutions in this study, the rotor must have a polar group, such as carboxyl in CCVJ to allow dissolving them.

The data show that the factor v in Equation 11 is not purely dye-dependent, but solution dependent as well. This is to be expected because many factors can affect the quantum yield, and thus the emission intensity, of any fluorescent dye. Particularly quenching effects caused by a change in the polarity of the environment need to be taken into account. It has been observed that molecular rotors react to a change in the environment's polarity with an emission wavelength shift, and to viscosity changes with a change in intensity [47,41]. Association of molecular rotors with hydrophobic pockets of proteins may remove the rotor from solvent contact, likely rendering it insensitive to the solution viscosity [32]. In our experiments, the Stokes shift for CCVJ varied very little between dextran and HES solutions, indicating that the rotor maintains significant aqueous contact and consequently that changes in the polarity of the environment are negligible. The idea that increased intensity is caused by non-covalent binding to the starch molecules can therefore be rejected. The most likely cause of variability in factor v is the sensitivity of the molecular rotor to free volume in its solvent. This shows the suitability of molecular rotors as non-mechanical viscosity sensors in aqueous solutions.

CHAPTER 3.

PRECISION ASSESSMENT OF BIOFLUID VISCOSITY MEASUREMENTS

USING MOLECULAR ROTORS

3.1. Introduction

To be successful as a technique for measuring blood viscosity, fluorescence viscometry must at least match the accuracy and precision of current instruments. The technique still relies on calibration by comparison with mechanical viscosity measurements, but the sensitivity and precision can be determined.

As previously mentioned, current instruments that apply shear have difficulty with blood and blood plasma. Earlier studies have examined the principle of molecular rotor viscosity sensitivity in mixtures of blood plasma with high-viscosity plasma expanders and in water-starch model systems [24,2].   No previous comparison of fluorescence viscometry precision using molecular rotors to currently available mechanical viscometers has been attempted.

In this study, we analyze the precision of two molecular rotors, 9-[(2-Cyano-2-hydroxy carbonyl)vinyl]julolidine (CCVJ) and 9-[(2-Cyano-2-hydroxy carbonyl)vinyl]julolidine triethyleneglycol ester (CCVJ-TEG) as viscosity sensors with respect to precision. Fluorescence viscometry results are compared with mechanical viscosity measurements.

3.2. Materials and Methods

Reagents obtained as follows: Fresh frozen human plasma was purchased from Interstate Blood Bank, INC. (Memphis, Tennessee), CCVJ from Helix Research (Springfield, OR), CCVJ-TEG was synthesized by our group [22], fluoroscopy grade dimethyl sulfoxide (DMSO) from Sigma (St. Louis, MO), Pentaspan (10% pentastarch in 0.9% NaCl, avg. MW 260 000) from B. Braun (Irvine, CA), Hetastarch (6% in 0.9% NaCl, avg. MW 670 000) from Abbott Laboratories (North Chicago, IL). Dextran (80 000 average MW) from Sigma (St. Louis, MO), was used to prepare 5% solution in physiologic saline. Fluorescence spectroscopy was performed with samples in 4 mL clear methacrylate cuvettes (Fisher Scientific; Pittsburgh, PA,) using Spex Fluoromax-3 (Jobin-Yvon; Stanmore, North London, UK). Absorbance measurements were made with a Beckman DU 520 spectrophotometer (Beckman Coulter, Fullerton, CA). Indices of refraction were taken with ATAGO R-5000 hand refractometer (ATAGO, Bellevue, WA).

Fresh frozen plasma was thawed prior to use, then centrifuged at 180 g for 15 minutes and filtered through 75 mm 0.22 µm SFCA filter (Nalgene, Rochestery, NY) to remove cryoprecipitate. Post-processing protein concentration was determined by refractometry and confirmed by Lowry method. Crystalline dye was dissolved in DMSO to make 20 mM stock solutions of CCVJ and CCVJ-TEG. Sample viscosity was modulated by varying the amount of unstained plasma mixed with the starch plasma expanders dextran, hetastarch, and pentastarch. Plasma prestained with CCVJ or CCVJ-TEG (67 µM) was

added in equal amounts to samples to minimize mixing errors. Final sample dye

concentration was 13.3 µM. Three milliliters of each sample were transferred to

4ml cuvettes and capped. All measurements were performed at room

temperature (24 °C).

Calibration sets consisting of 5 different viscosities and 5 replicates each

were made according to Table 4. A test set of 5 plasma-pentastarch mixtures,

with different viscosity values than the calibration set, was made separately with

3 replicates each.

Physical viscosity measurements for plasma mixtures were made with Brookfield

Table 4: Calibration set consisted of 5 replicates of 5 plasma-plasma
expander ratios with 13.3 µM dye.

Sample Set	Plasma (ml)	Expander (ml)	Prestained Plasma (ml)
1	4	0	1
2	3	1	1
3	2	2	1
4	1	3	1
5	0	4	1

DV-III+ (Middleboro, MA) cone-plate viscometer with a CPE-40 spindle. Samples

of 0.5 ml were measured at discrete shear rates: 150, 300, 450, 600, and 750 s^{-1},

(20, 40, 60, 80, and 100 rpm) in a ramp-up, ramp-down series. Viscosity

measurements were taken at 80 rpm (600 s^{-1}). This shear rate was chosen to

remain within instrument accuracy limits, and to reduce any apparent non-

Newtonian effects on results. While noticeable instrument fluctuations as well as

apparent shear-thinning effects existed at shear rates of 300 s^{-1} and below, no

aparent influence of shear rate on measured viscosity existed at 450 s^{-1} and

above.

Reference viscosity η_{ref} was computed for each plasma-plasma expander

combination using Eq. 15 [55],

$$\ln \eta_{ref} = \sum_{i=1}^{n} w_i \cdot \ln \eta_i \qquad (15)$$

where η_i is the viscosity of the individual component as measured by cone-plate

viscometer and w_i is the fractional amount of n=2 components, plasma and

expander. We verified this equation and found it excellently described the

plasma/expander mixtures, as represented in Fig. 14
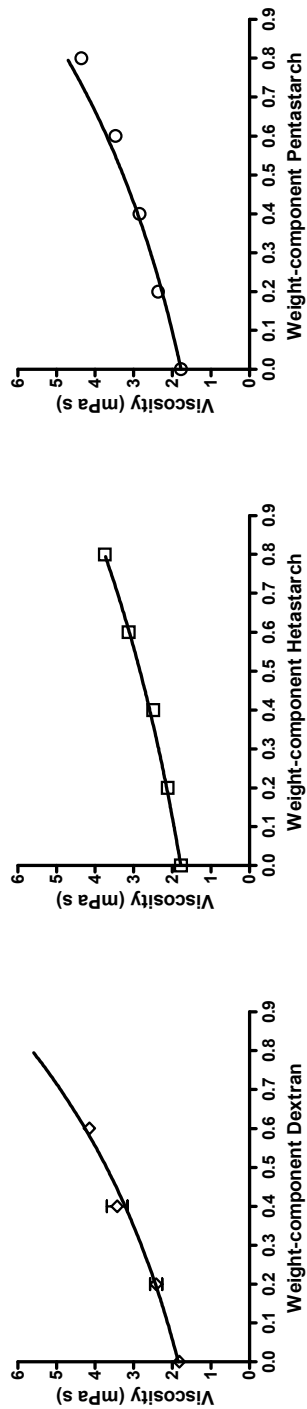
Figure 14: Reference viscosity (line) of plasma-hetastarch mixture computed using Eq. 15 from mechanically measured viscosity at 24°C (data points). Error bars indicate standard deviation.

The fluorescence emission intensity of each sample was measured from 470-530 nm at excitation wavelength of 440 nm for CCVJ, and 460 nm for CCVJ-TEG. Excitation and emission slits were 2 nm with integration time of 0.5 s. Peak intensity per sample was computed by averaging the emission intensity in a 5 nm window centered on the emission peak. Using the known relationship between viscosity η and quantum yield φ of a molecular rotor, Equation 16 [18]:

$$\log \phi = C + x \log \eta \qquad (16)$$

we solved the above equation for η, which yielded the fluorescence-based vicsosity η_F. The constant $\kappa \propto 10^{-C}$ relates quantum yield and dye concentration and $v = 1/x$ describes the viscosity sensitivity of the molecular rotor:

$$\eta_F = (\kappa \cdot I)^v \qquad (17)$$

Constants κ and v were determined from linear regression of log intensity over log viscosity for each plasma-expander calibration set. Deviation, d of η_F from the reference viscosity, η_{ref} was computed using the following equation:

 Fluorescence intensities of the test set samples were measured in the same manner as the calibration set. For each sample, η_F was computed according to

Eq. 17, using the constants ν and κ derived from the calibration set of plasma and pentastarch mixtures. The cone-plate viscometer was also used to measure sample viscosities. Deviation from η_{ref} was calculated for both η_F and viscometer results using Eq. 18. Absorption measurements at 440nm and 490nm were used

$$ d = \frac{\eta_F - \eta_{ref}}{\eta_{ref}} \cdot 100\% \qquad (18) $$

to normalize dye concentration between calibration set and individual test samples. A standard concentration factor was determined from the calibration set by linear regression of absorbance at 440nm (A_{440}) versus absorbance at 490nm (A_{490}), where the slope (χ) is related to plasma absorbance, and the intercept (β) is directly related to dye concentration. A normalization factor (Δ) was calculated for each sample according to Equation 19. Normalized intensity was determined by multiplying measured sample intensity by the factor Δ.

$$ \Delta = \frac{A_{440} - \chi \cdot A_{490}}{\beta} \qquad (19) $$

3.3. Results

3.3.1. Cone-Plate Viscometer

Physical viscosity values of human blood plasma at the shear rates used are represented in Fig. 15, with standard deviation shown by error bars. Viscosity

curves for plasma-hetastarch mixtures are shown in Fig. 16 and are typical of all

plasma-plasma expander mixtures. Deviations between viscosity measurements

at 60 rpm and 100 rpm were less than 4% for plasma-hetastarch mixtures, 8%

for plasma-dextran mixtures, and 5% for plasma-pentastarch mixtures.
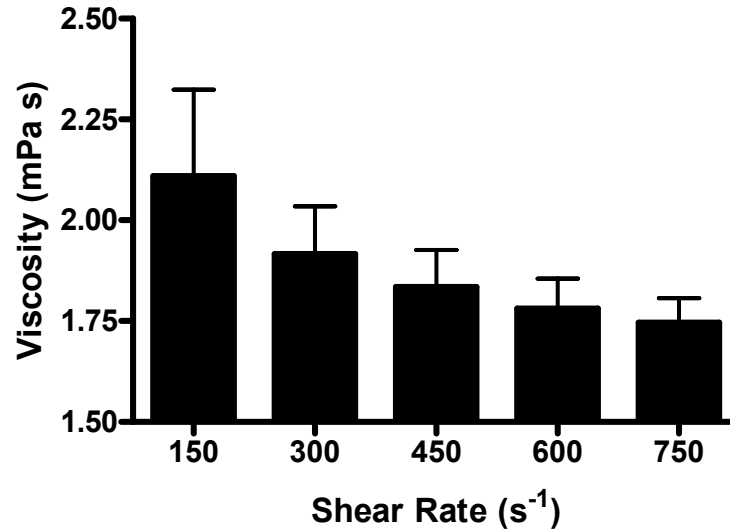
Figure 15: Error analysis of blood plasma viscosity as measured using cone-plate viscometer at indicated shear rates at 24°C. Error bars indicate standard deviation. Deviation is lower and non-Newtonian behavior is minimal at higher shear rates.

3.3.2. Refractance

Indices of refraction varied from 1.349 for pure plasma to 1.348 for pentastarch

solution. According to Lakowicz, the correction factor for intensity is $(n_i/n_0)^2$,

where n_i is the sample and n_0 is air [39]. This would lead to a difference of less

than 0.3% of fluorescence intensity values (counts per second) between plasma

and pentastarch solution. The influence of refractive index change was therefore

neglected in spectroscopic measurements.
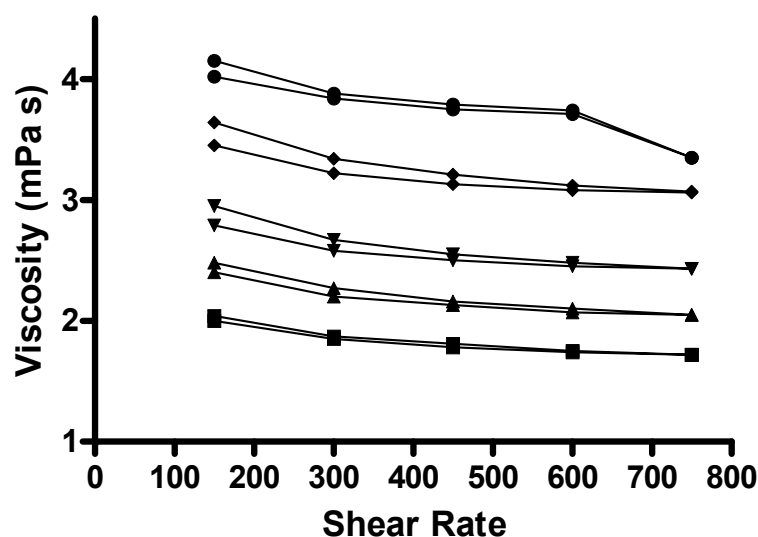
Figure 16: Viscosity values for plasma-hetastarch mixtures obtained with cone-and-plate viscometer at various shear rates using ramp-up, ramp-down protocol showing non-newtonian behavior of plasma. The highest viscosity solution exceeded instrument limits at 750 s^{-1}.

3.3.3. Absorbance

Figure 17 shows the absorption spectra of plasma and a plasma-pentastarch mixture with and without CCVJ. The contribution of the dye to the total absorbance is highest in the range of 430-450 nm, and is negligible at 490 nm and above. By measuring absorbance at the excitation peak of the dye (around 440 nm) and near the emission peak (490 nm), it is therefore possible to separate the contribution of the fluid and the dye towards total absorbance. This separation can be used to normalize the fluorescence intensities of a test set to that of the calibration set according to dye concentration as measured by absorbance (Fig. 18).

49
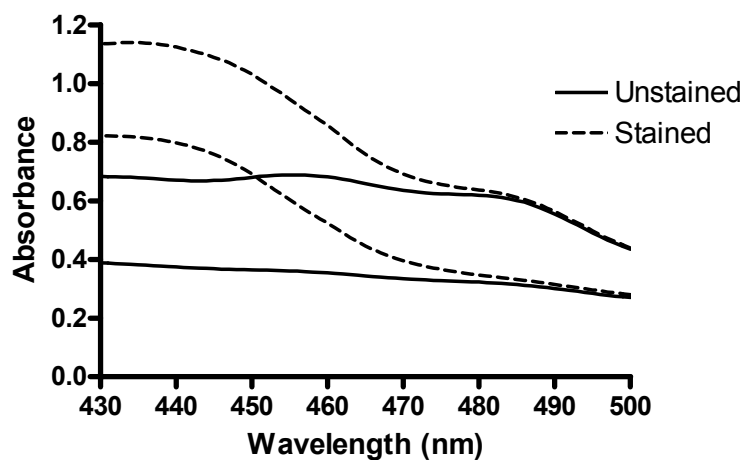
Figure 17: Absorption spectra of CCVJ stained and unstained plasma-pentastarch mixtures. Solution absorbance at 490nm and above is attributable to plasma alone, not dye.
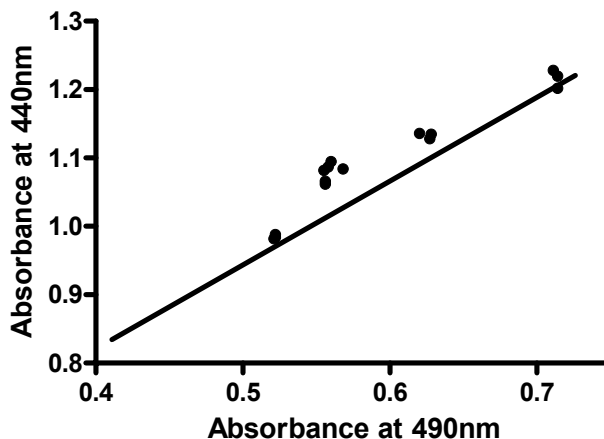
Figure 18: Sample absorbance compared with calibration set absorbance (line) for dye concentration normalization. The slope the line is related to plasma absorbance, and the intercept is directly related to dye concentration. The correction factor Δ is calculated according to Eq. 19.

3.3.4. Molecular rotor fluorescence

Both CCVJ and CCVJ-TEG dissolved completely in the plasma mixtures. Plasma autofluorescence did not significant affect fluorescence measurements at the dye concentration used in this study. Average wavelength of peak emission was 476 nm for CCVJ and 498 nm for CCVJ-TEG at excitation wavelength of 440 nm and 460 nm, respectively, with less than 5nm deviation. Figure 19 shows the comparison of log CCVJ fluorescence intensity to log plasma-hetastarch viscosity.
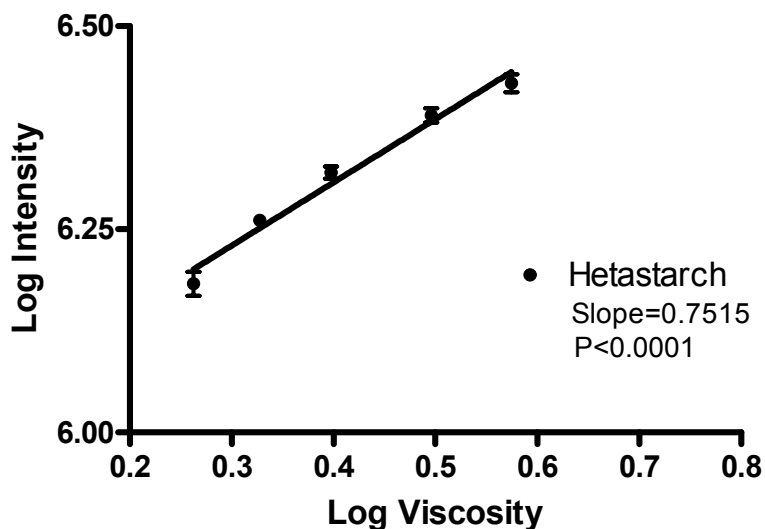
Figure 19: Log-log comparison of CCVJ fluorescence vs. plasma-hetastarch mixture viscosity. Error bars indicate standard deviation.

Table 5: Comparison of average percent deviation from viscosity calibration curve for viscosity measurements made with cone and plate viscometer and fluorescence viscometry with molecular rotors. Percent deviation is reduced by the absorbance correction method using Eq. 19.

Sample	Cone and Plate	Fluorescence Viscometry	
		Before Correction	After Correction
1	-2.61	-0.28	-2.31
2	-5.05	2.21	-3.83
3	-4.08	8.81	-2.38
4	-1.82	6.78	-3.13
5	0.08	3.67	1.07
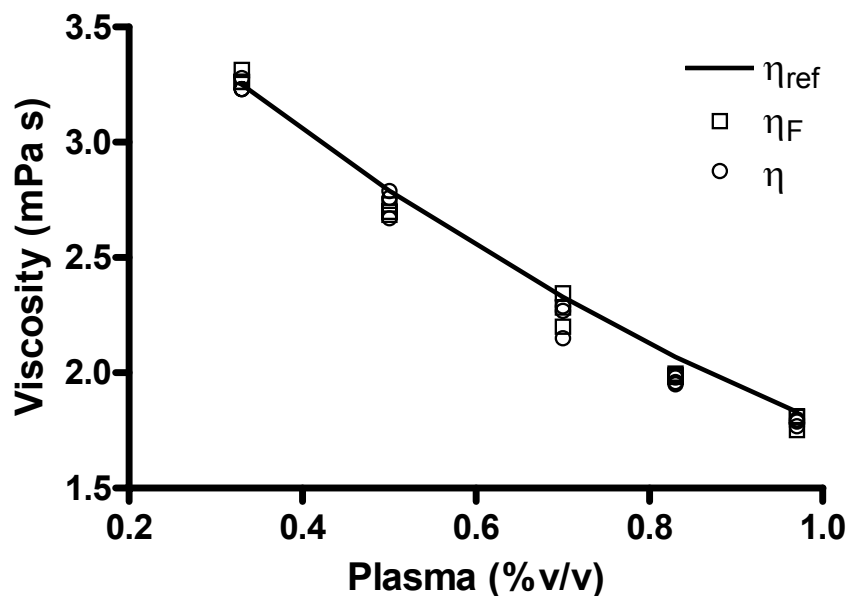
Figure 20: Comparison of viscosity measurements made by cone-plate viscometer with fluorescence viscometry from calibration curve.

Tables 6 and 7 list the calibration constants κ and v for Eq. 17 for the calibration sets stained with CCVJ and CCVJ-TEG, respectively. These tables also show that back-calculation of viscosity from molecular rotor fluorescence within the calibration set, using Eq. 17, resulted in deviation of less than 10% for all samples.

Coefficients of variation for mechanical and fluorescence viscosity measurements are compared for hetastarch, pentastarch and dextran in Tables 10, 8 and 9, respectively.

For the test set, viscosity determined by fluorescence η_F of dissolved CCVJ in plasma-pentastarch mixtures was compared with values of η_{ref} as determined by Eq. 15 for the plasma-pentastarch calibration set (Fig. 20). Maximum deviation for physical viscosity measurements using the cone-plate viscometer was 5.1% (Table 5) With normalization of test set dye concentration to the calibration set (Eq. 19), deviation of η_F was reduced from greater than 8% to less than 4% (Table 5).

Table 6: Constants of Eq. 17 for CCVJ in plasma-plasma expander mixtures with maximum deviation.

Plasma Expander	κ	v	Max Deviation
Hetastarch (6%)	0.0049	0.639	4.9%
Pentastarch (10%)	0.0036	0.703	5.03%
Dextran (5%)	0.0032	0.454	3.75%

Table 7: Constants of Eq. 17 for CCVJ-TEG in plasma-plasma expander mixtures with maximum deviation.

Plasma Expander	κ	v	Max Deviation
Hetastarch (6%)	0.0013	0.9684	5.48%
Pentastarch (10%)	0.00369	0.6959	3.20%
Dextran (5%)	0.00279	0.4391	1.32%

Table 8: Comparison of coefficients of variation of mechanical and fluorescence viscosity measurements of plasma-pentastarch mixtures with CCVJ and CCVJ-TEG.

Viscosity	Mechanical Coefficient of Variation	CCVJ Fluorescence Coefficient of Variation	CCVJ-TEG Fluorescence Coefficient of Variation
Average	0.022	0.024	0.02
1.7	0.049	0.03	0.02
2.14	0.021	0.029	0.016
2.7	0.015	0.029	0.009
3.41	0.025	0.008	0.038
4.3	0.001	0.022	0.015

Table 9: Comparison of coefficients of variation of mechanical and fluorescence viscosity measurements of plasma-dextran mixtures with CCVJ and CCVJ-TEG.

Viscosity	Mechanical Coefficient of Variation	CCVJ Fluorescence Coefficient of Variation	CCVJ-TEG Fluorescence Coefficient of Variation
Average	0.062	0.019	0.012
1.63	0.051	0.015	0.016
1.77	0.086	0.009	0.01
1.92	0.1	0.024	0.01
2.16	0.069	0.023	0.012

Table 10: Comparison of coefficients of variation of mechanical and fluorescence viscosity measurements of plasma-hetastarch mixtures with CCVJ and CCVJ-TEG.

Viscosity	Mechanical Coefficient of Variation	CCVJ Fluorescence Coefficient of Variation	CCVJ-TEG Fluorescence Coefficient of Variation
Average	0.028	0.022	0.022
1.78	0.049	0.044	0.034
2.13	0.035	0.018	0.016
2.5	0.018	0.012	0.018
3.13	0.022	0.018	0.02
3.75	0.019	0.018	0.025

3.4. Discussion

Mechanical viscosity measurement poses significant limitations. Relatively large sample volumes are required, and the measurement process is time-consuming. With biofluids, protein deposits at the surface may be particularly difficult to remove, adding to the time necessary to clean the instrument between samples. Furthermore, blood plasma has apparent non-Newtonian properties due to a surface layer formed by proteins [58]. Total protein content of the plasma sample used in this study was 6.6 g/dL, which is above average protein concentration for human plasma. Plasma protein concentration contributes directly to viscosity and may affect viscosity measurements at low shear rates [58]. Selection of the proper shear rate is critical. Often viscosity is estimated from models of non-Newtonian fluids, since it

is currently impossible to measure viscosity without applying shear.

3.4.1. Method comparison

Advantages of fluorescence viscometry over current physical viscometers include: rapid analysis, shear-less measurement, and no cleaning due to disposable cuvettes. Four hours were required to complete mechanical viscosity measurements for a batch of 25 samples, while fluorescence measurements of the same samples took about 30 minutes including warm-up and calibration of the fluorometer.

Spectroscopic measurement of fluorescence can be done with very small sample sizes, dependent on the equipment used. Disposable microcuvettes with sample volumes less than 100µl are available commercially for fluorescence spectrophotometry. Disposable cuvettes would allow quick testing and disposal of samples with minimal exposure of instrument operator to potentially infectious biological fluids.

Mechanical precision depended on completely removing protein adhered to the stainless steel surfaces of the cone and plate between samples. Brookfield recommends yearly maintenance of the viscometer, including replacement of the jewel bearing necessary for smooth rotation of the cone. The bearings slowly wear out, reducing accuracy and precision during use of the instrument. Vigorous use of the instrument speeds the necessity for bearing replacement. The instrument manufacturer recommends yearly offsite

maintenance which means added expense and bench time lost. The cone-and-plate viscometer allows small fluid sample size (500µl), but for the reasons mentioned is not practical for processing multiple samples in short time-periods as necessary in the clinical setting.

3.4.2. Precision comparison

The viscosity values obtained by measurement with the viscometer are not the true viscosities of plasma. In our measurements, plasma exhibited apparent non-Newtonian properties (Fig. 16) which may be explained by the formation of a surface protein layer [9]. Shear of biofluids may result in rearrangement of the molecules in solution, distorting the viscous properties. The protein layer is likely a large source of error between measurements of solution of the same composition. For this reason, measured viscosity was adjusted to η_{ref} to reduce error associated with the cone-plate viscometer. While we compared fluorescence viscometry with the cone-plate viscometer, no instrument can be held as a gold standard at this time.

While viscosity is related to quantum yield (Eq. 16), fluorescence intensity is also related to dye concentration even in highly absorbing solutions [31]. The method of fluorescence viscometry proposed uses fluorescence intensity measurements, not quantum yield, and is thus susceptible to errors caused by small variations in dye concentrations. Calculating viscosity from intensity necessitates either very accurate addition of dye to the solution of interest or the ability to correct for variations in dye concentrations. We have shown that the

58

effect of minor differences in dye concentration can be minimized using additional absorption measurements at the excitation and emission wavelength of the molecular rotor used (Eq. 19). Fluorescence intensity can be normalized to a standard by relating the concentration of a test sample to that used in a calibration set, which greatly improves the precision of this method (Table 5). Using this normalization, we found that fluorescence-based viscosity measurements were possible with the same precision (less than 4% deviation from the theoretical values) as measurements based on a cone-and-plate instrument (about 5% deviation from the theoretical values). To directly compare precision, deviations in each set were expressed by the coefficient of variation, a scaling-independent metric. Average coefficients of variation (Tables 8-9).

Experimental results from this study show that the determined slopes for both dyes exceed the theoretical value of 2/3. This result may be explained by the absorption of the plasma-plasma expander mixtures. Plasma has a higher optical density than plasma expander solutions, which have absorbance very close to that of water. In our previous study [2] of molecular rotors in transparent starch solutions, the determined slopes were close to or below the theoretical value. The same solutions were used in this study to modulate plasma viscosity, with the secondary effect of slightly altering optical properties. Therefore, with addition of transparent plasma expander solution, observed fluorescence intensity increased due to changes in both viscosity and optical density, resulting in larger slopes of log-log plots (x of Eq. 16). A further correction step will be necessary to compensate for these changes in optical density, such as used in

this study (Eq. 19). Alternatively, plasma expanders could be manufactured with an optical density close to that of plasma, thus minimizing this error.

It is known that both viscosity and fluorescence are temperature dependent qualities. Rheometry using fluorescent molecular rotors will be significantly affected by temperature differences, since intramolecular rotation rate is temperature dependent. Maintaining temperature at a set value for all samples should avoid such problems, as in this study. If it is not possible to control sample temperature, it is likely the method can be calibrated for temperature changes with simultaneous temperature measurement. Viscosity as measured by molecular rotors would need to be adjusted according to the temperature at time of measurement, just as with current viscometers.

3.5. Conclusions

Biofluid viscosity measurement using fluorescent molecular rotors has great potential for clinical application. As discussed in a previous study [2], the method must be calibrated for the specific expander solution used. Calibration constants were determined for CCVJ and CCVJ-TEG in mixtures of plasma and three common colloid additives, dextran, hetastarch, and pentastarch. Results show that by calibrating for the specific components, fluorescence viscometry can be used to determine the viscosity of a complex mixture with high precision.

Further study of the interaction between macromolecules such as those found in blood plasma and other biofluids is necessary to better understand the mechanisms of molecular rotors as mechanosensors in complex fluid mixtures.

Blood plasma protein concentrations can vary significantly between individuals

and may influence molecular rotor fluorescence characteristics.

CHAPTER 4.

INTERACTION OF FLUORESCENT MOLECULAR ROTORS WITH BLOOD PLASMA PROTEINS

4.1. Introduction

For clinical use, fluorescence viscometry must be insensitive to normal inter-patient variations of biofluid component concentrations, specifically plasma proteins. Blood plasma is an aqueous solution of proteins and electrolytes. Plasma proteins such as albumin are known to bind to various pharmaceuticals in the bloodstream. Albumin has higher affinity for hydrophobic molecules than hydrophilic molecules due to hydrophobic "pockets" in the protein structure [14]. Protein binding inhibits the availability of the drug to the rest of the body by preventing its escape from blood vessels [52]. The normal plasma concentration ranges of three of the most prevalent proteins in human blood plasma: albumin, fibrinogen and immunoglobulin G (IgG), are listed in Table 11.

The hydrophobic molecular rotor DCVJ has been used to probe hydrophobic pockets and conformational changes of proteins such as bovine calmodulin [33] and actin [32]. In purely aqueous media, DCVJ is insoluble and precipitates due to its hydrophobic properties. In the presence of protein, strongly reduced crystal formation has been observed.

Newly developed hydrophilic molecular rotors are soluble in aqueous solutions, but still are more soluble in less polar solutions such as ethylene glycol

and methanol [22]. We hypothesize that molecular rotor-protein association via hydrophobic pockets decreases fluid viscosity sensitivity. Therefore, molecular rotors with lower binding affinity for plasma proteins would be most effective as clinical blood plasma viscosity sensors. In this study, molecular rotor binding with common blood plasma proteins was examined by equilibrium dialysis and relative binding affinities at various protein concentrations compared.

4.2. Materials and Methods

Materials obtained as followed: DCVJ and 9-[(2-Cyano-2-hydroxy carbonyl)vinyl]julolidine (CCVJ) were purchased from from Helix Research (Springfield, OR), CCVJ-triethylene glycol ester (CCVJ-TEG), CCVJ-diethylene glycol ester (CCVJ-DEG) and p-[(2-cyano-2-propanediol ester)vinyl]dimethylaniline (Diol) were synthesized by our group [22]. Fluoroscopy grade DMSO was purchased from Sigma (St. Louis, MO), bovine serum albumin (BSA, Fraction V, Heat Shock Isolation; Biotechnology Grade) from Midwest Scientific (St Louis, MO), fibrinogen (Fraction I type I-S from bovine plasma) and bovine IgG (technical grade in 0.01 M phosphate buffered saline, pH 7.2 with 15 mM sodium azide as preservative) from Sigma (St. Louis, MO) and fresh frozen human plasma from Interstate Blood Bank, Inc. (Memphis, Tennessee). Bovine plasma proteins were used in this study due to their similarity of structure and function to human plasma proteins. Becton Dickinson polypropylene conical tubes, 13 mm nylon syringe filters (0.2 μm pore size), 1.5 ml polypropylene flat top microcentrifuge tubes, and flat bottom polystyrene 96-

well microplates were purchased from Fisher Scientific, (Pittsburgh, PA), cellulose membrane dialysis tubing (10 mm flat width, 12,000 to 14,000 nominal molecular weight cutoff) from Sigma (St. Louis, MO) and from Fisher Scientific (Pittsburgh, PA).

Protein concentrations used were chosen to approximate molecular rotor interaction at physiologic plasma concentration of the specific proteins. Proteins may interact differently in simple aqueous solutions than in plasma and other complex biofluids. Quantitative information obtained by through such experiments may not apply in natural situations.
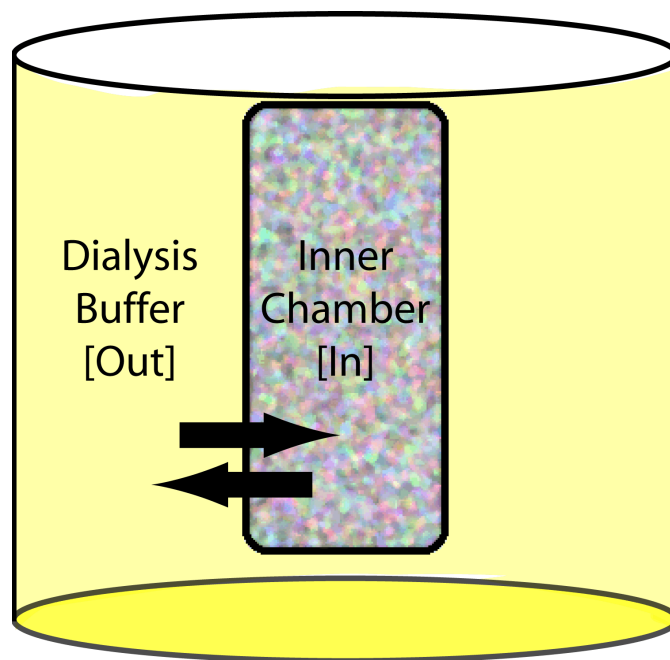
Figure 21: Schematic of equilibrium dialysis setup. Molecular rotors diffuse from the dialysis buffer in the outer chamber through the size-restrictive dialysis membrane into the inner chamber. Proteins dissolved in the inner chamber solution are prevented from diffusing across the membrane. With sufficient time, an equilibrium is reached between the two chambers. Dye concentration in each chamber is dependent on its protein affinity.

DCVJ powder was dissolved in DMSO to make a 1 mM stock solution. Crystalline BSA varying from 0.5 mg to 3.0 mg was measured into individual microcentrifuge tubes. Ten µl of DCVJ stock solution were added to each before dissolving completely in 1.0 ml saline buffer (0.9% sodium chloride solution with 15 mM sodium azide to prevent bacterial growth.) Samples were allowed to stand closed in microcentrifuge tubes for 8 hours at 23 °C then were filtered individually to remove dye crystals. Dye concentration was determined by absorption spectroscopy at 455 nm, then compared to protein concentration determined by Bio-Rad DC colorimetric assay (Bio-Rad, Hercules, CA). Protein concentration was assayed after filtration to account for any loss due to filtration. The resulting solution consisted of dissolved dye and protein.

Solutions of BSA and fibrinogen were made by dissolving the crystalline proteins in saline buffer. Bovine IgG and human plasma solutions were prepared by diluting with saline buffer. Stock 20 mM dye solutions were made by dissolving crystalline dye in DMSO. Dialysis buffers were made by adding stock dye solution to 0.9% saline to make 3 µM solutions of CCVJ and Diol and 4 µM solutions of CCVJ-TEG and CCVJ-DEG. All dialysis buffers were made fresh the day of use.

The diffusion rate of dyes from the dialysis buffer across the dialysis membrane was analyzed. Ten aliquots of 500 µL protein-free, unstained saline buffer were loaded in separate three-inch sections of dialysis tubing and clipped securely at both ends, one end weighted. Clips were placed to minimize dead space inside the dialysis chamber. Each sample was completely immersed in 30

mL of dialysis buffer containing the dye of interest in separate 50 mL polypropylene centrifuge tubes. The tubes were capped tightly and placed inside an incubator at 37 °C. Absorbance measurements were performed using a Molecular Devices UVmax kinetic microplate reader (Sunnyvale, CA). Initial inner unstained saline buffer and outer buffer solution containing dye were analyzed for dye concentration by absorbance at 440 nm for CCVJ and Diol, and at 460 nm for CCVJ-DEG and CCVJ-TEG before dialysis. Absorbance at 490 nm was used as the background reference for all dyes because they absorb minimal light at that wavelength [3]. Two 200 µL aliquots were removed from each sample and placed in separate wells in a microplate at times 0.5, 1, 1.5, 4 and 7 hours after beginning dialysis. These sampling times allowed characterization of the diffusion curves for all dyes and determination of equilibration time.

The protein samples were treated similarly, except dialysis occurred over 20 hours to allow the dye to completely equilibrate across the dialysis membrane and associate with the protein. One 30 mL aliquot of dialysis buffer was incubated in the same manner to serve as a blank for dye concentration. After dye equilibration, two 200 µL samples were withdrawn from the dialysis tubing and two 200 µL samples were also withdrawn from dialysis buffer. Samples were placed in microplate wells and scanned for absorbance at 440 nm, 460 nm, and 490 nm.

Protein solution absorbances were also measured at the same wavelengths for the concentrations used in the dialysis experiments. Absorption coefficients were calculated and used to correct sample absorbance for protein

content. The ratio of protein-bound to free dye R_{Pr}, was calculated using Eq 20 for comparison of each dye-protein combination:

$$R_{Pr} = \frac{A_i - A_{Pr}}{A_0} \qquad (20)$$

where A_i is the sample absorbance, A_{pr} is the light absorbance by protein and A_0 is the dialysis buffer absorbance.

Dye absorbance in plasma was determined by subtracting sample absorbance at 490 nm from absorbance at 440 nm for CCVJ and Diol or 460 nm for CCVJ-TEG and CCVJ-DEG. The plasma bound dye ratio, R_{Pl} was determined using Eq 21 where A_λ is the appropriate wavelength for the dye used.

$$R_{Pl} = \frac{A_\lambda - A_{490}}{A_0} \qquad (21)$$

Two regression models, linear and nonlinear, were tested for all molecular rotor-protein combinations. The nonlinear model tested was a hyperbolic, one-site binding model according to Eq 22, where B_{max} is the maximal binding and K is the concentration of molecular rotor necessary for half of maximal binding. Both models were compared with the F-test to determine the best fit model. Regression analyses were performed using GraphPad Prism version 4.01 for Windows, GraphPad Software, San Diego California.

$$Y = \frac{B_{max} \cdot X}{(K + X)}$$
Equation **(22)**

4.3. Results

Protein-bound DCVJ concentration was plotted against the sample protein concentration (Fig. 22). The binding relationship best adheres to the one-site binding model as determined by F-test as described above. The concentration of DCVJ relative to BSA concentration in the 5% solutions was about 0.6 mg DCVJ to 1 mg BSA, which comes out to be about 150 molecules DCVJ per protein molecule. Dye concentrations reached equilibrium across the dialysis membrane within 7 hours for all dyes (Fig. 23). Dye adsorption onto the membranes was negligible and sample volumes remained constant.

Plots of ratio versus protein concentration for the dyes used are shown for albumin (Fig. 24), fibrinogen (Fig. 26) and IgG (Fig. 25). Regression analysis of the data indicated a linear relationship between protein concentration and dye binding affinity for IgG and fibrinogen for all dyes ($P<0.01$). Dye binding with BSA followed the one-site binding model (Eq. 22) for CCVJ, CCVJ-TEG and CCVJ-DEG ($P<0.01$). As the protein concentration was increased relative to the dye concentration, the binding ratio approached an asymptote. The binding ratios for specific proteins and for plasma in the normal physiologic ranges predicted by regression analysis are presented in Table 11, as well as the percent change expected over the protein concentration range. Predicted variations of dye binding ratios over physiologic concentration ranges for all proteins were 11% or

less for CCVJ, CCVJ-DEG and CCVJ-TEG. Diol dye binding ratios were lower and variation higher than ratios for other dyes ($P<0.01$) and better fit a linear model for all proteins including albumin ($P<0.01$).

Total plasma protein of the human plasma sample used was 6.3 g/dL, (normal is 6.5 to 8.3 g/dL in healthy humans [44]) as determined by Bio-Rad DC colorimetric assay (Bio-Rad, Hercules, CA). Plasma retention of dye followed trends similar to that of the albumin samples, but with significantly higher protein binding ratios (Fig 27). Predicted plasma binding ratios were less than 10% for all dyes over the normal protein range.
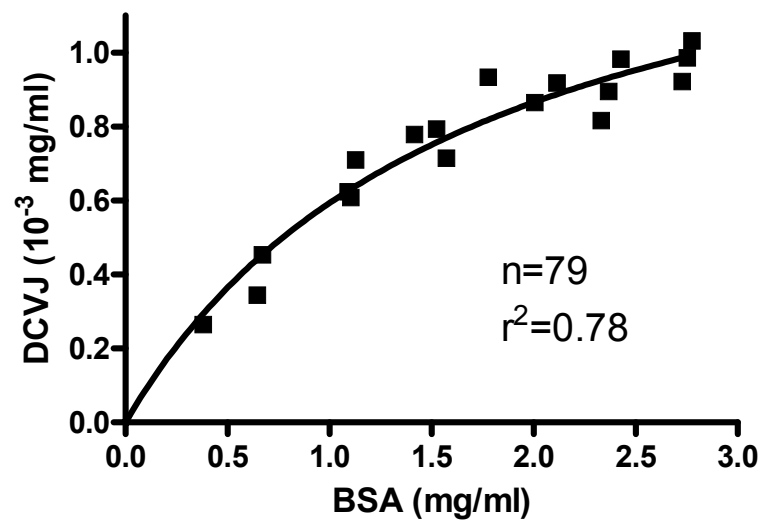
Figure 22: DCVJ binding to bovine serum albumin. DCVJ and BSA concentrations determined by spectroscopy after filtration of samples.
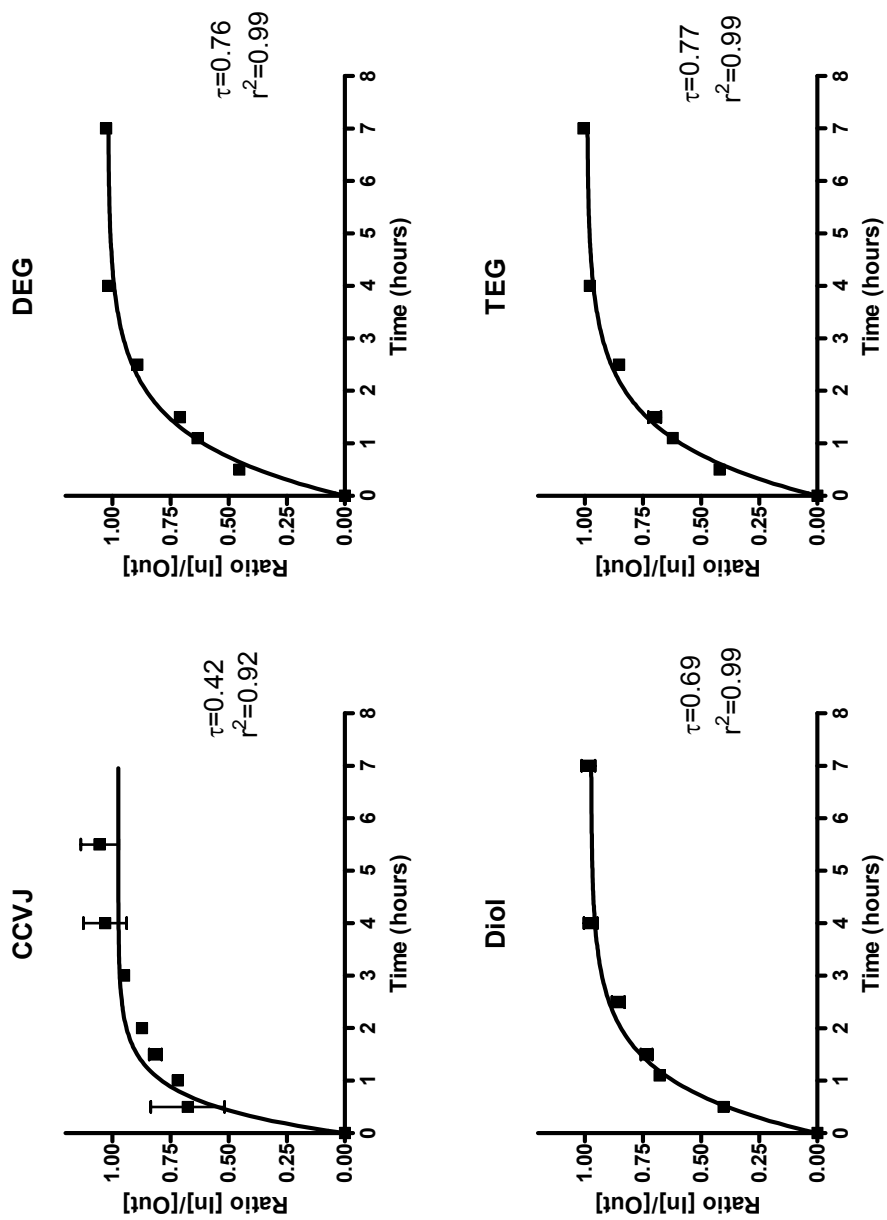
Figure 23: **Diffusion.** Molecular rotor diffusion from outer dialysis buffer to inside dialysis chamber fit to exponential model: $Y = Y_{max} * (1 - \exp(-K_d * t))$ where K_d is the rate of diffusion into the chamber and the half time (τ) is $0.69/K_d$. Dye adsorption to membrane was negligible. Each data point represents the mean of 2 replicates with error bars for standard deviation.
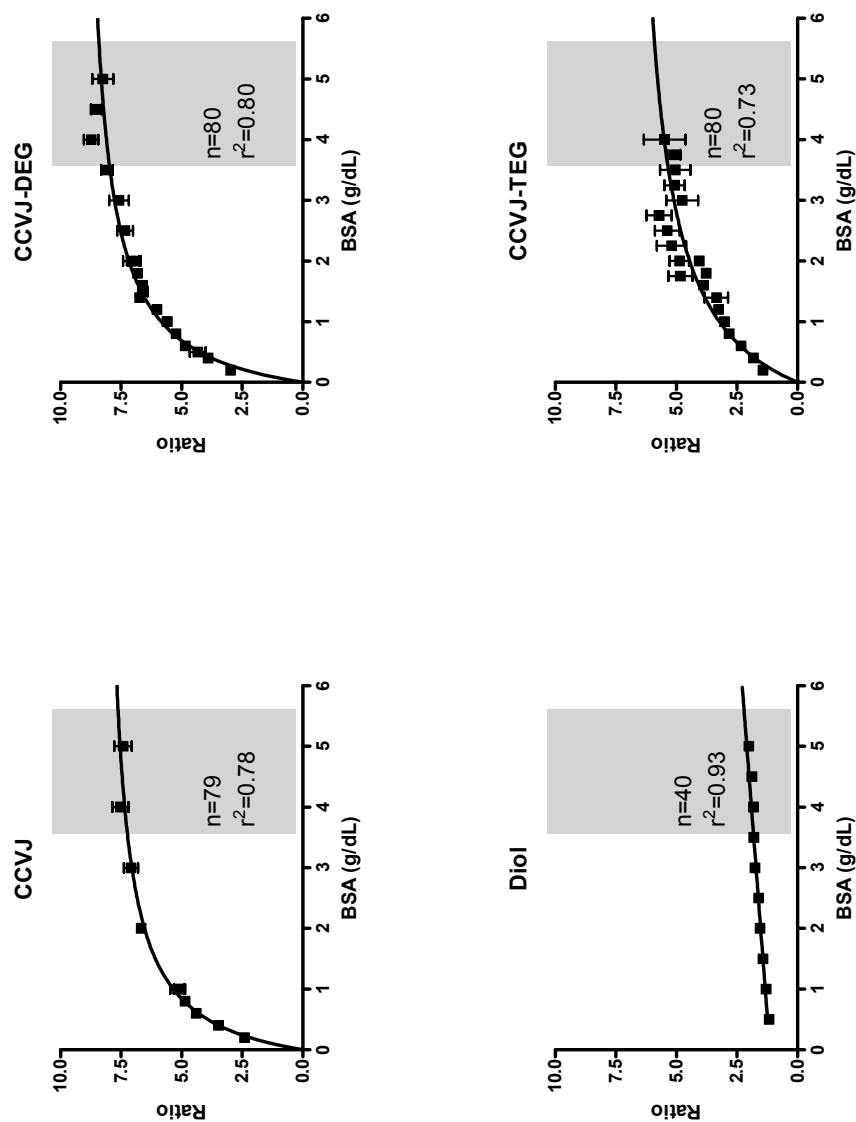
Figure 24: **Albumin [3.5-5.5 g/dL]**. Comparison of relative binding affinities of molecular rotors to albumin. The Y-axis represents the ratio of bound to unbound dye calculated from Eq 20. The shaded area represents the normal plasma protein concentration in healthy individuals. Diol affinity for albumin is significantly less than other dyes and showed a linear binding relationship rather than hyperbolic. Each data point represents the mean of at least 4 replicates with error bars for standard deviation.
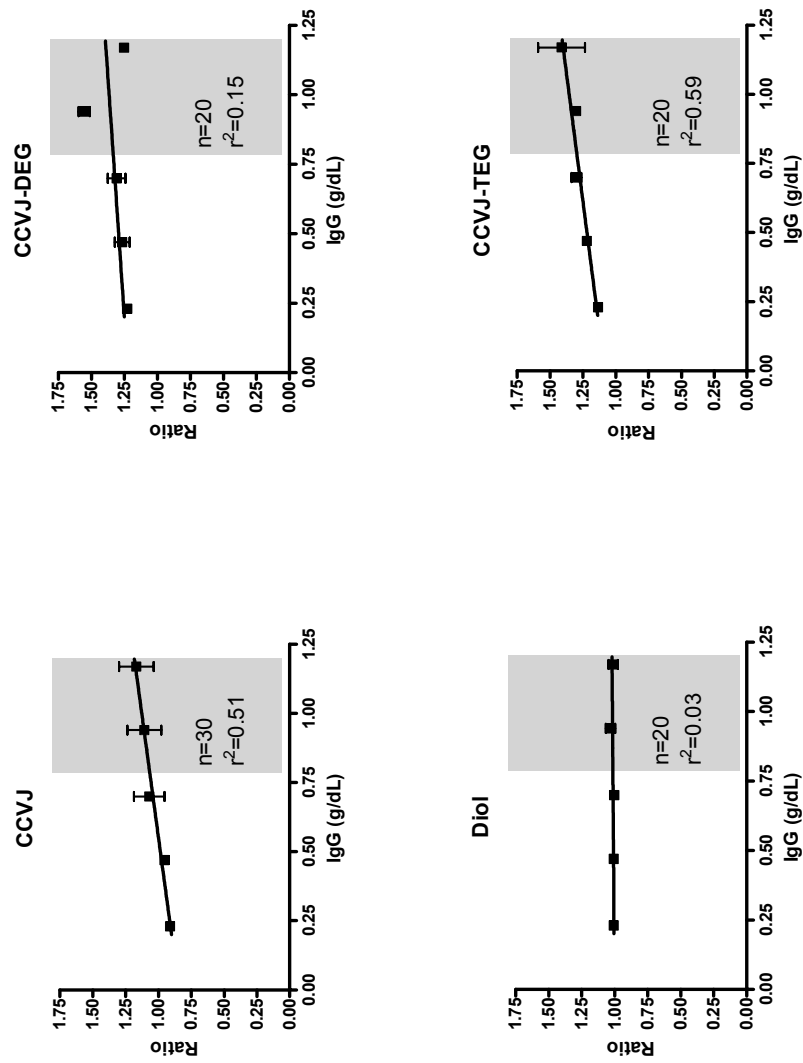
Figure 25: **IgG [0.8-1.2 g/dL]**. Comparison of relative binding affinities of molecular rotors to IgG with relative slopes and r squared values. The Y-axis represents the ratio of bound to unbound dye calculated from Eq 20. The shaded area represents the normal plasma protein concentration in healthy individuals. The slopes for CCVJ-DEG and Diol are not significantly non-zero (P>0.05), and correlations (r squared values) between binding ratio and protein concentration are close to zero. Each data point represents the mean of 4 replicates with error bars for standard deviation.
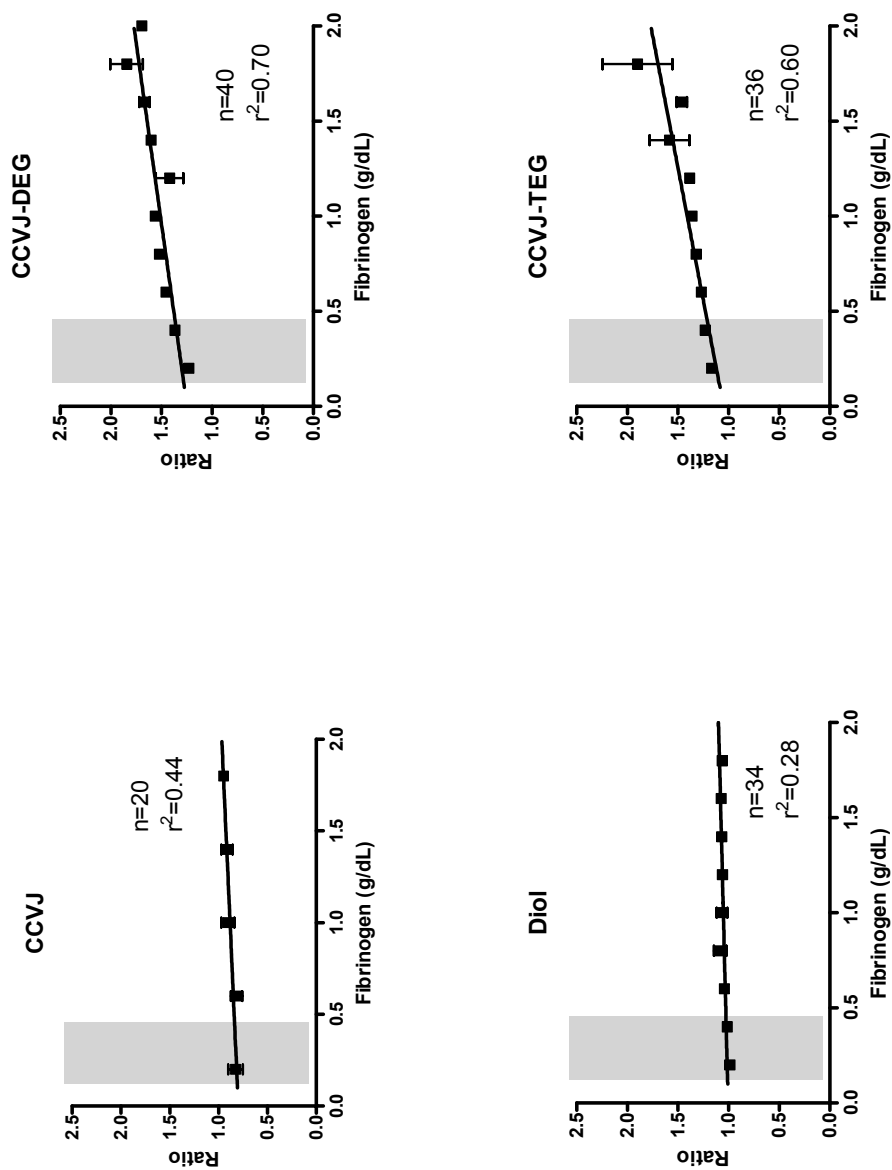
Figure 26: **Fibrinogen [0.2-0.45 g/dL].** Comparison of relative binding affinities of molecular rotors to fibrinogen with relative slopes and r squared values. The Y-axis represents the ratio of bound to unbound dye calculated from Eq 20. The shaded area represents the normal plasma protein concentration in healthy individuals. Each data point represents the mean of 4 replicates with error bars for standard deviation.
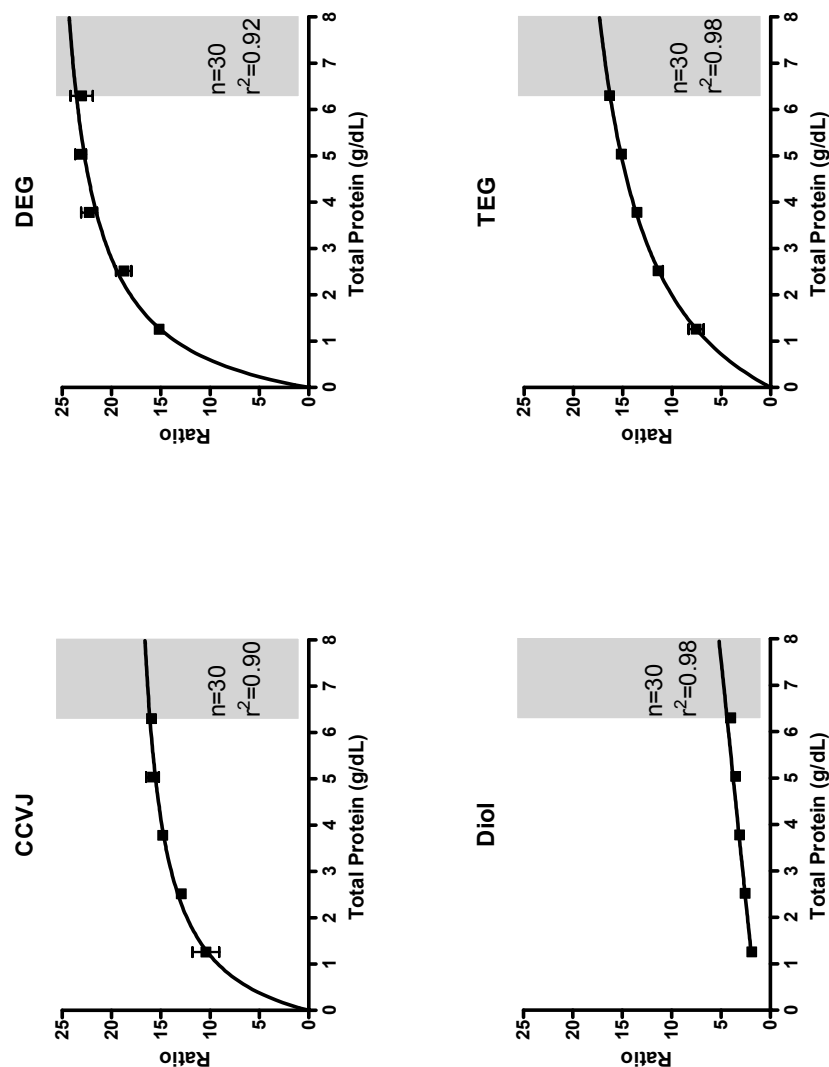
Figure 27: Human Plasma [6.5-8.3 g/dL]. Comparison of relative binding affinities of molecular rotors in human blood plasma. The Y-axis represents the ratio of bound to unbound dye calculated from Eq 21. The shaded area represents the normal plasma protein concentration in healthy individuals. The best curve fit was determined by linear regression and nonlinear regression with one-site binding model (Eq 22) and subsequent F-test for best fit. Diol binding to plasma was less than the other three and best fit a linear model. Diol appears to be the best choice of the molecular rotors tested for viscosity measurement of protein-containing biofluids. Each data point represents the mean of 4 replicates with error bars for standard deviation.

75

Table 11: Protein Binding Ratios. Relative binding ratios of molecular rotors with specific blood plasma proteins as determined by Eq 20. Physiologic concentration is given in [g/dL] for each protein and for plasma protein content for healthy human subjects. Binding ratios as predicted by regression models are reported for the lower and upper protein concentration ranges with percent deviation in parentheses. Molecular rotor binding was most significant for albumin.

Molecular Rotor	Albumin [3.5-5.5 g/dL]	Fibrinogen [0.2-0.45 g/dL]	IgG [0.8-1.2 g/dL]	Human Blood Plasma [6.5-8.3 g/dL]
CCVJ	7.2-7.6 (5.6%)	0.82-0.84 (2.4%)	1.1-1.2 (9.0%)	16.2-16.7 (3.1%)
CCVJ-DEG	8.0-8.4 (5.0%)	1.3-1.4 (7.6%)	1.3-1.4 (7.6%)	23.7-24.4 (3.0%)
CCVJ-TEG	5.3-5.9 (11%)	1.1-1.2 (9.0%)	1.3-1.4 (7.6%)	16.4-17.6 (7.3%)
Diol	1.8-2.1 (17%)	1.0-1.0 (0%)	1.0-1.0 (0%)	4.5-5.4 (20%)

4.4. Discussion

Proteins present in human blood plasma complicate mechanical viscosity measurement. Current viscometers must shear fluid samples to measure viscosity, which may alter the physical properties of biofluids [9]. Human blood plasma viscosity measurement using the fluorescent molecular rotors CCVJ and CCVJ-TEG has been shown to be practical, with precision equal to or greater than that of a cone and plate viscometer [3]. Human blood plasma samples vary in electrolyte and protein concentration from patient to patient. The purpose of this study was to determine the extent of molecular rotor interaction with common plasma proteins so corrective measures may be developed to minimize the effect of patient-to-patient variations on fluorescence viscosity measurement of plasma. Molecular rotor-protein interaction is assumed to be via hydrophobic pockets similar to pharmaceutical-protein binding [14], but other mechanisms may be present.

This study compared the relative binding affinity of four fluorescent molecular rotors to the most abundant blood plasma proteins with the binding affinity of dyes in human blood plasma by equilibrium dialysis. Equilibrium dialysis is a commonly used method to determine plasma protein binding ratios [52]. The membrane restricts movement of proteins, while molecules of molecular weight less than 10,000 freely diffuse through it. Dialysis was used in this study in preference of other methods because absolute quantification of dye binding was not necessary. Relative binding affinities (Rpr of Eq 20) of specific proteins were obtained for comparison. A ratio above 1 indicates a greater

concentration of dye inside the dialysis tubing than in the dialysis buffer. Greater concentration inside indicates affinity of dye for protein is greater than for solvent.

The results show albumin is the primary protein in plasma that associates with the dyes. For CCVJ, CCVJ-DEG and CCVJ-TEG, the predicted proportion of bound dye changes 5.6%, 5.0% and 11% respectively, in the normal physiologic albumin concentration range (Table 11). This indicates that small changes in protein concentration will not affect the total amount of bound dye, and thus the measured fluorescence of the dye. The amount of dye bound and, according to our hypothesis, isolated from the solvent, will remain at a constant level. Molecular rotor concentration will need to be above this threshold to achieve solvent viscosity sensitivity. In the albumin solutions, this threshold appears to be about 8 times the CCVJ dialysis buffer concentration of 3 µM, which would be 24 µM.

In plasma, the ratios for healthy plasma range (6.5-8.3 g/dL) is much higher than for albumin solutions. Plasma is a complex mixture of proteins and other components which may interact with the dyes. Also, the ratio method was slightly different for the optically dense plasma solutions than the clear simple protein solutions (Eq. 21), which may have artifactually resulted in elevated binding ratios.

For CCVJ, CCVJ-TEG and CCVJ-DEG the nonlinear trend infers an asymptote near the physiologic protein concentration. Prediction of the variation between binding ratios at the low and high ends of normal plasma protein concentrations shows less than 10% difference for CCVJ, CCVJ-DEG and

78

CCVJ-TEG for all experiments (Table 11). Predicted variation for Diol was much greater (20%), but showed much lower binding ratio values. Despite the higher variability, the lower binding ratios for Diol show more dye is not associated with protein in simple protein solutions or in plasma. Unbound dye can be considered freely dissolved in the plasma and sensitive to solvent viscosity.

A notable trend presents that indicates molecular rotor structure is very important to protein binding. CCVJ-TEG has only one more ethylene glycol subunit than CCVJ-DEG, but CCVJ-TEG has lower binding affinity. Diol is the most hydrophilic of the molecular rotors tested and has the lowest affinity for albumin, close to its affinity for the other proteins.

4.5. Conclusion

It is apparent from this study that changes in plasma protein levels within the physiologic range do not greatly affect the absolute free dye concentration, and thus the sensitivity of molecular rotors for viscosity measurement. For all dyes, simple models can be developed to predict protein interaction over various concentrations. Molecular rotor structure is very important in protein-binding affinity. DCVJ is insoluble in pure aqueous solutions, but solubility increases with protein concentration. Hydrophilic molecular rotors are more soluble in aqueous solutions and have lower affinity for proteins. Results of this study indicate more hydrophilic molecular rotors are better suited for sensing viscosity in biofluids such as blood plasma because they show less protein interaction. Further studies are needed to determine how protein binding affects molecular rotor

viscosity sensitivity. Development and investigation of more hydrophilic molecular rotors such as Diol will lead to improved biofluid viscosity measurement using fluorescent molecular rotors.

CHAPTER 5.

SURFACE-IMMOBILIZED MOLECULAR ROTORS FOR FLUID VISCOSITY

MEASUREMENT

5.1. Introduction

Surface-immobilized fluorescent molecular rotors were used as the sensing element in a fiber-optic viscosity sensor. Previous studies have proven the viscosity sensitivity of molecular rotors dissolved in ethylene glycol-methanol mixtures and viscosity-modulated aqueous colloid and colloid-blood plasma mixtures. A fiber-optic probe with immobilized molecular rotors would be better suited for small sample biofluid viscosity measurement. A fiber-optic sensor would allow remote light sensing and would not require addition of dye to fluid samples.

Optical fibers conduct light through total internal reflection. Total internal reflection occurs when light traveling in a material encounters a boundary with a material of lower refractive index ($n_2 < n_1$) at an angle $\alpha_C > \sin^{-1}(n_2/n_1)$. Optical fibers consist of a high refractive index core surrounded by a lower refractive index cladding. Single mode fibers transmit only a small bandwidth of light while multimode fibers may accept light in broader range of wavelengths and angles of transmission.

A conical-tapered fiber tip acts as a mode-converter, converting excitation light to higher order modes (larger angle with respect to core-cladding interface) for better evanescent wave excitation of surface-bound fluorophores and

converting accepted fluorescence light to lower order modes for better propagation through the optical fiber [20]. The reflection of light from the inner surface at distance z in the tapered tip is given by Eq. 23. Fig. 28 shows how light transmission in the taper acts as a mode converter.

$$r(0)\sin\alpha(0) = r(z)\sin\alpha(z) \qquad\qquad \textbf{(23)}$$
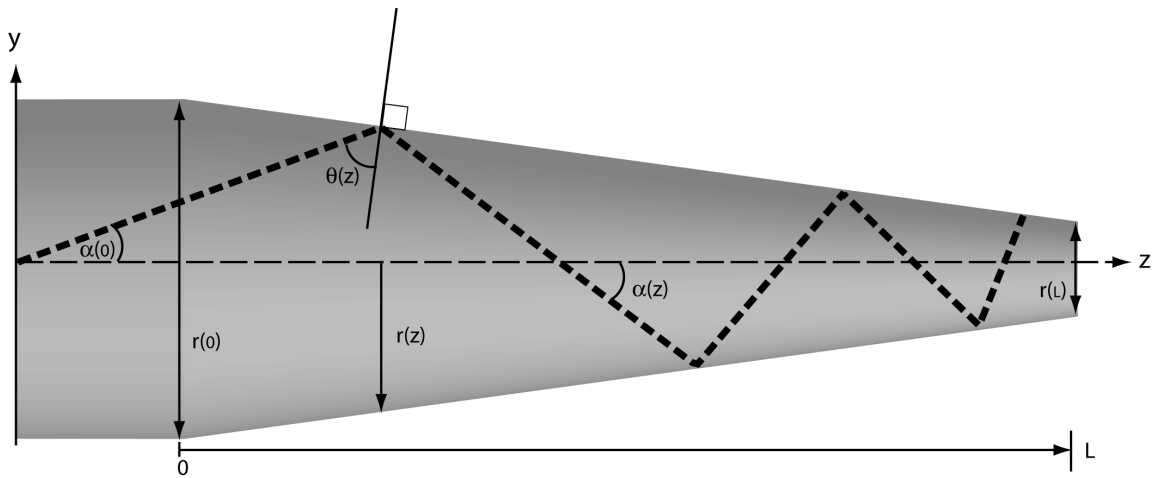
Figure 28: Tapered optical fiber tip acts as a mode converter, increasing the power of evanescent wave excitation and improving fluorescence collection efficiency. (Redrawn from [20]).

Functionalization of fiber optic and nanoparticle surfaces by immobilization of sensing molecules has been used to create sensors for detection of bacteria [7], toxins [35] and other molecules [28,56,53]. One popular method of covalently attaching molecules to a glass surface uses organosilanes such as n-[3-(trimethoxysilyl)propyl]-ethylenediamine (AENPS) and 3-aminopropyl-triethoxysilane (APTES), (Fig. 30) [37,17]. The triethoxysilyl groups react with

hydroxyl groups on the glass surface (Fig. 31). The terminal amino groups react with succimidyl groups added to the fluorescent molecules (Fig. 29) in a second step (Fig. 32).

CCVJ fluorescence was compared to immobilized fluorescein fluorescence in 5 ethylene glycol-methanol mixtures varying in viscosity from 7 mPa s to 14mPa s.

AENPS   APTES
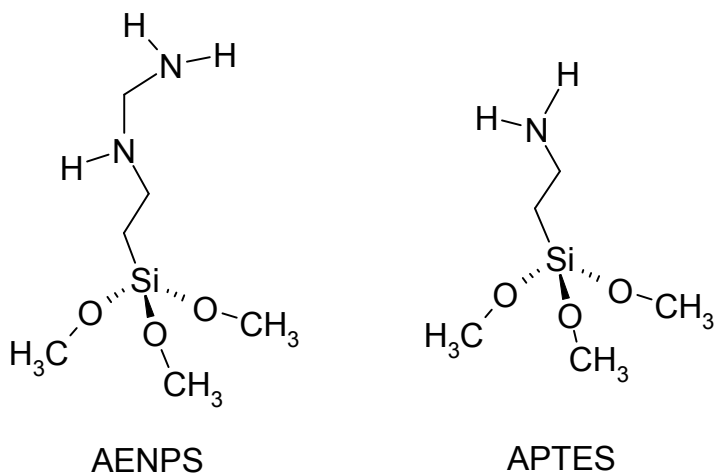
Figure 30: Organosilanes 3-aminopropyl-triethoxysilane (APTES) and n-[3-(trimethoxysilyl)propyl]-ethylenediamine (AENPS) .

CCVJ-NHS   CCVJ-TEG-NHS
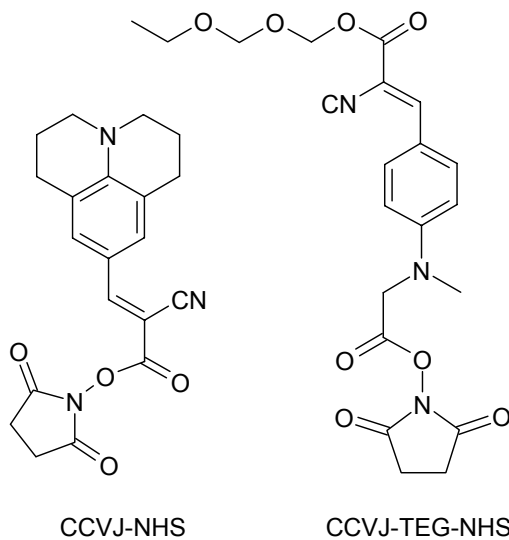
Figure 29: Molecular rotors CCVJ and CCVJ-TEG with succimidyl ester active groups. Succimidyl group is attached to the cyano side of CCVJ while it is on the ring side of CCVJ-TEG.
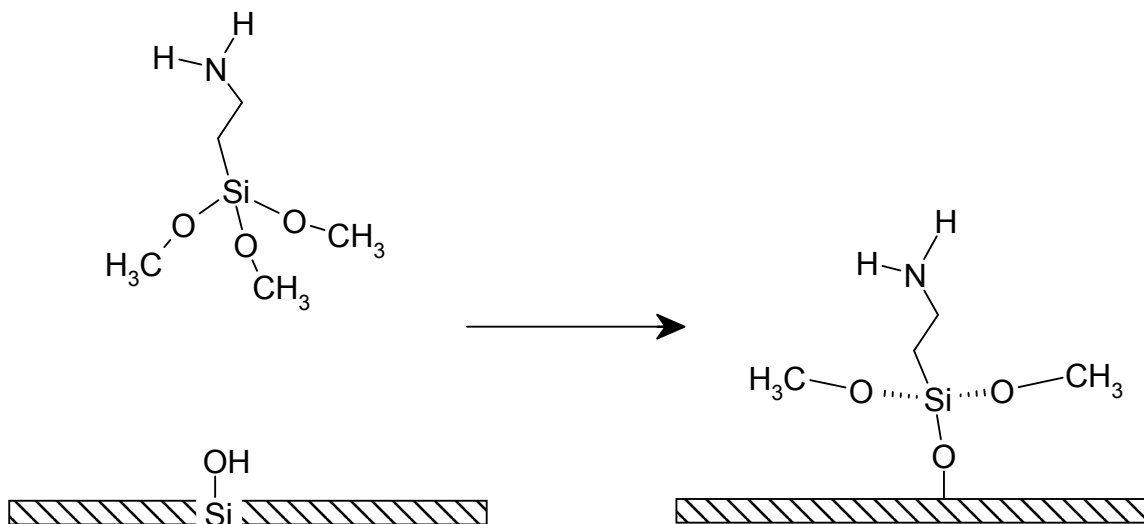
Figure 31: Representation of silane film attachment to glass surface. Siloxyl bonds are substituted for the surface hydroxyl groups on the prepared glass surface.
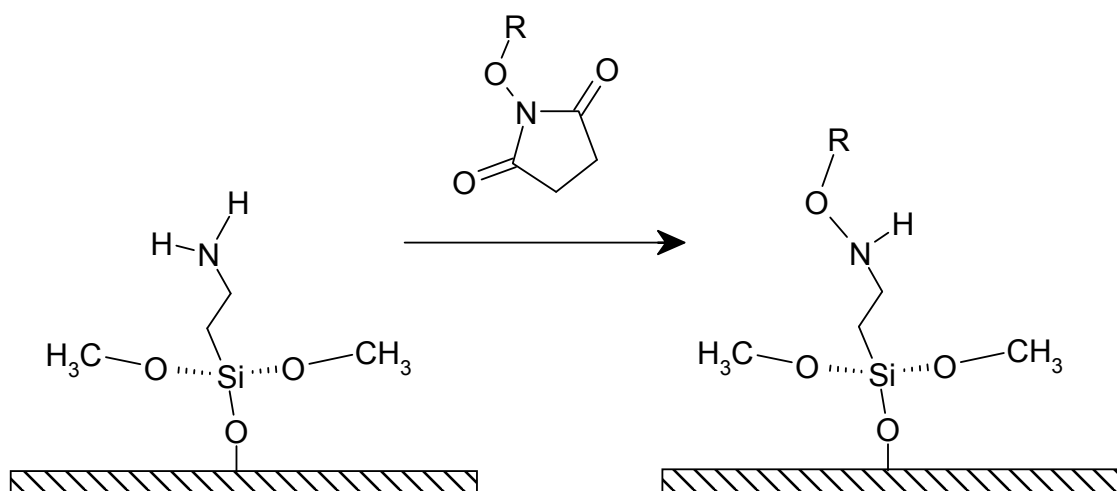
Figure 32: Covalent binding of molecular rotor (R) to amino end of organosilane by reaction with succimidyl group.

5.2. Materials

CCVJ succimidyl ester (CCVJ-NHS) purchased from Helix Research (Springfield, OR), Fluorescein-NHS from Molecular Probes (Eugene, OR) and CCVJ-TEG-NHS synthesized by our group were stored at -20°C. Silica dioxide nanopowder (15nm average particle size), APTES, AENPS, methanol, acetone, ethylene glycol from Sigma-Aldrich (St. Louis, MO). Pure fused-silica core with fluorine-doped cladding, step-index multimode 600 μm core, 0.22 numerical aperture diameter optical fibers were purchased from Ocean Optics (Dunedin, FL), 15 ml polypropylene centrifuge tubes, methylacrylate 4 ml cuvettes and 1.5 ml semi-microcuvettes from Fisher Scientific (Pittsburgh, PA). Absorbance measurements were conducted with Beckman DU 520 spectrophotometer, (Beckman Coulter, Fullerton, CA,) and fluorescence measurements with Jobin-Yvon Spex Fluoromax-3 (Stanmore, North London). Hermle Z200A centrifuge (Hermle-Labortechnik, Germany). Indices of refraction were taken with ATAGO R-5000 hand refractometer (ATAGO, Bellevue, WA).

5.3. Methods

5.3.1. Surface Preparation

The jacketing was stripped from the distal 1.5cm of each fiber and etched with hydrofluoric acid (HF) using a custom micro-controlled mechanical system to form 1 cm long 1° tapers. Tip surfaces were visually examined under magnification for defects. Glass nanoparticles were used as received from the

manufacturer without further preparation.

5.3.2. Surface Functionalization

Stock 1mg/ml DMSO solutions of succimidyl esters of CCVJ (Helix Research, Springfield, OR), CCVJ-TEG (synthesized by our group) and fluorescein were made immediately prior to use.

Functionalization of optical fibers was performed in duplicate for each experiment using fibers labelled 1a and 2a or 1b and 2b. Fiber tips were prepared prior to silanization by immersing in 40% hydrofluoric acid (HF) for 5 minutes, then sulfuric acid (H2SO4) for 30 minutes, then 1:1 MeOH:HCL for 30 minutes with double distilled water (ddH2O) rinses between and after. Tips were then immersed in boiling ddH2O for 30 minutes to activate the glass surface and allowed to dry. Each fiber tip was then immersed in 2% by volume APTES or AENPS (Fig. 30) in acetone for 1 hours, then rinsed in acetone and allowed to dry. Next, 75 µl stock dye solution were added to 400 ul 50 mM sodium bicarbonate buffer, pH 8.5 in a 500 µl centrifuge tube and vortexed. The fiber tip was inserted immediately and soaked for 2 hours. The tip was then rinsed well in acetone and air dried.

Silica nanoparticles (0.2g) were sonicated in 20 ml 2.0% APTES solution in acetone for 1 hour, then centrifuged for 15 min at 1500g and the supernatant discarded. The particles were rinsed in 20 ml acetone and sonicated 2 hours to redisperse. Nanoparticles were separated into 4-4ml aliquots, then centrifuged again, 15 min at 1500g, the supernatant discarded, and the particles dried

overnight. 150 µl of stock dye solution was added to dry silanized nanoparticles, pure DMSO was used for control experiments. Next, 8 ml 50 mM Na_2CO_3, pH 8.5 was added, vortexed, then sonicated for 2 hours, centrifuged 15 min at 1500g, and the supernatant discarded. The nanoparticles were sonicated in 10 ml acetone, centrifuged 15 min at 1500g, and the supernatant discarded for two rinses, then dried overnight.

5.3.3. Fluorescence Measurement

Fluorescent measurements were performed with fiber-optic probe and nanoparticles tested in ethylene glycol-methanol mixtures with final concentrations of 0, 5%, 10%, 15% and 20% methanol in ethylene glycol (Table 12) and aqueous dextran solutions of varying viscosities. Labeled nanoparticles
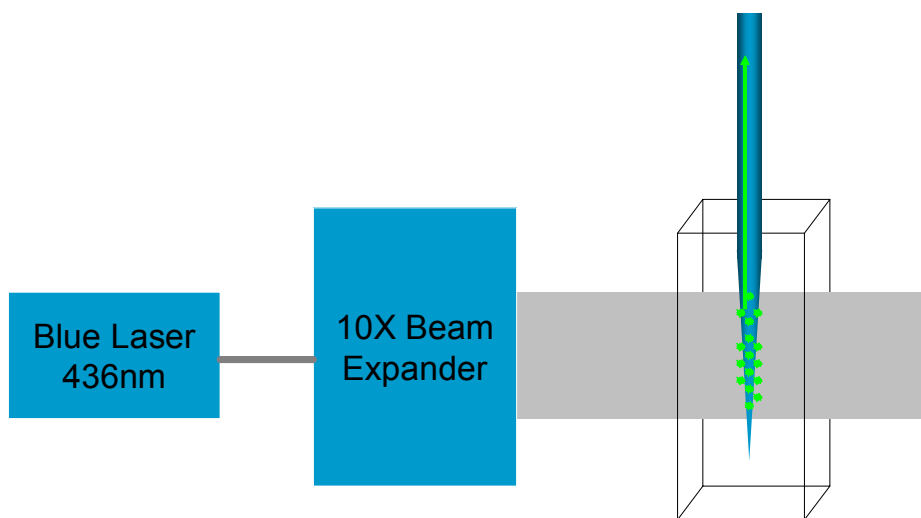
Figure 33: Setup for external excitation of fluorescent molecules covalently bound to the surface of tapered optical fiber.

were also tested in mixtures of 5%, 10%, and 15% glycerol in ethylene glycol.

The proximal end of the fiber was attached to a custom fiber-optic stage in a spectrofluorometer for internal illumination and fluorescence emission detection. The distal tapered end of the fiber was held by fiber chuck and custom cuvette holder and the tip immersed in the fluid of interest contained in a clear methylacrylate cuvette. A 440 nm blue laser with 10X beam expander was used for external illumination (Fig. 3). Spot size for the beam was about 1 cm.

Table 12: Experimental setup and physical characteristics of samples.

Sample	Methanol	Viscosity	n
0	0	13.35	1.429
1	5	11.39	1.424
2	10	9.71	1.419
3	15	8.28	1.414
4	20	7.06	1.409

Fluorescence was measured for each fiber with alternating external and internal illumination. Internal excitation was at 440 nm with 2 nm slits. Emission intensity was scanned from 470 nm to 550 nm in 1 nm increments.

Labeled silica nanoparticles were resuspended in 10 ml ethylene glycol by 2 hours of sonication. Test samples were made by combining 300 μl nanoparticle suspension with ethylene glycol-methanol mixtures with final concentrations of 0, 5%, 10%, 15% and 20% methanol in ethylene glycol. A second experiment was performed with mixtures of 0, 5%, 10% methanol in ethylene glycol and 5%, 10% and 15% glycerol in ethylene glycol. Samples were made in triplicate in semi-

microcuvettes. Light absorbance of control samples used in these experiments was 0.13 at 500 nm.

Control and fluorescein nanoparticle suspensions were excited at 440 nm with 2nm slits for excitation and emission. CCVJ and CCVJ-TEG samples were excited at 440 nm and 460 nm respectively, with 4 nm slits for excitation and emission. The emission signal was scanned to adequately characterize peaks between the excitation wavelength and 550 nm with integration time of 0.5 s for all measurements.

5.4. Results

The measured fluorescence intensity of immobilized molecular rotors did not correlate significantly with aqueous dextran solution viscosity. Molecular rotors immobilized to AENPS film did not retain fluorescence sensitivity.

5.4.1. Fiber-optic Probe

Fluorescence intensity for internal illumination was greater than external by nearly a factor of 10, with broad peaks. Linear regression was performed for the normalized fluorescence intensity versus the ethylene glycol-methanol mixture viscosity. Fluorescence intensity measured using the fluorescein fiber-optic probe did not change significantly with solution viscosity (P>0.05) for external excitation, while immobilized CCVJ and CCVJ-TEG fluorescence increased with solution viscosity (P<0.01) for both external (Fig. 35) and internal illumination (Fig. 34). The slopes and r^2 values determined by linear regression

fiber-optic probe results are reported in Table 13.

Table 13:Results of linear regression analyses of normalized intensity versus sample viscosity for fiber-optic probes.

Label	External		Internal	
	Slope	r^2	Slope	r^2
Fluorescein	NS	NS	0.004	0.47
CCVJ	0.061	0.91	0.021	0.9
CCVJ-TEG	0.005	0.039	0.002	0.74
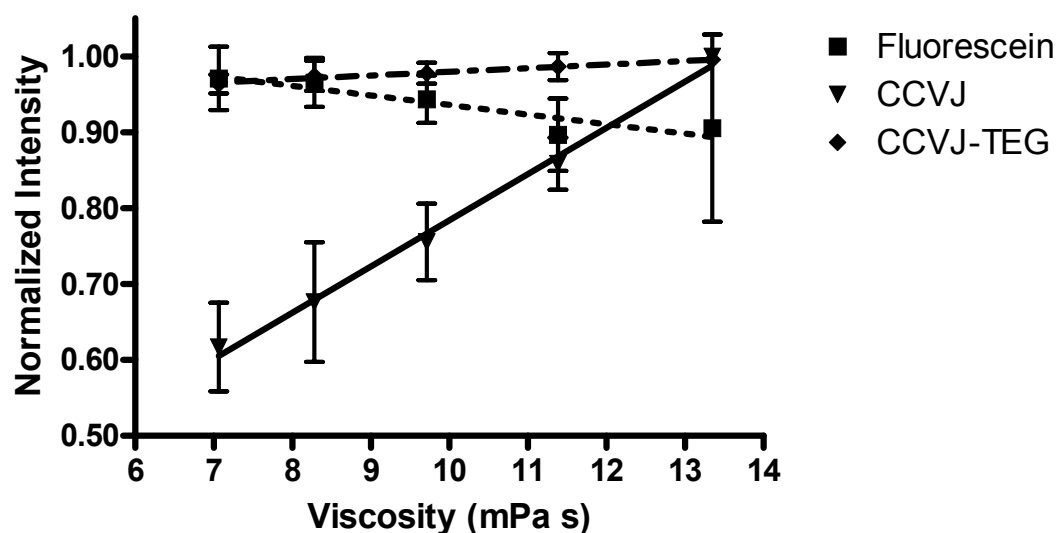
Figure 35: Plot of log intensity vs. log viscosity for CCVJ, CCVJ-TEG and fluorescein immobilized on the surface of tapered optical fibers with external illumination by 440 nm blue laser with 1 cm beam diameter.
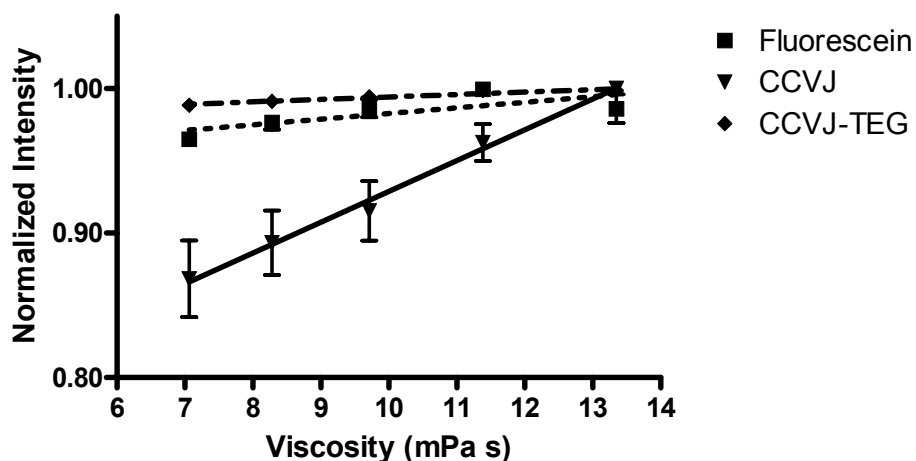
Figure 34: Plot of log intensity vs. log viscosity for CCVJ and Fluorescein immobilized on the surface of tapered optical fibers with filtered arc lamp illumination from the proximal end attached to the spectrofluorometer.

5.4.2. Nanoparticles

Figures 37 and 36 represent the emission spectra of CCVJ-NHS and CCVJ-TEG-NHS in ethylene glycol, respectively, compared to their surface-immobilized counterparts. The emission peak for CCVJ changed from 510 nm free to 500 nm immobilized. The CCVJ-TEG peak showed a red shift upon immobilization, from 495 nm to 520 nm.

The log of sample peak emission intensities were compared to the log of sample viscosities for the control samples (Fig. 38) and for labeled samples (Fig. 39). Fluorescein and unlabeled nanoparticle emission signal negatively correlates with solution viscosity while CCVJ and CCVJ-TEG emission is positively correlated with sample viscosity. Results of linear regression analyses are listed in Table 14 with the average percent difference in emission intensity per step increase in sample viscosity.

Table 14:Results of linear regression analyses of log of peak intensity versus log of sample viscosity for labeled silica nanoparticles.

Label	λ_{peak} (nm)	Slope	r^2	%change
Fluorescein	520	-0.29	0.85	-4
CCVJ	500	0.45	0.96	8.2
CCVJ-TEG	520	0.27	0.89	4.6
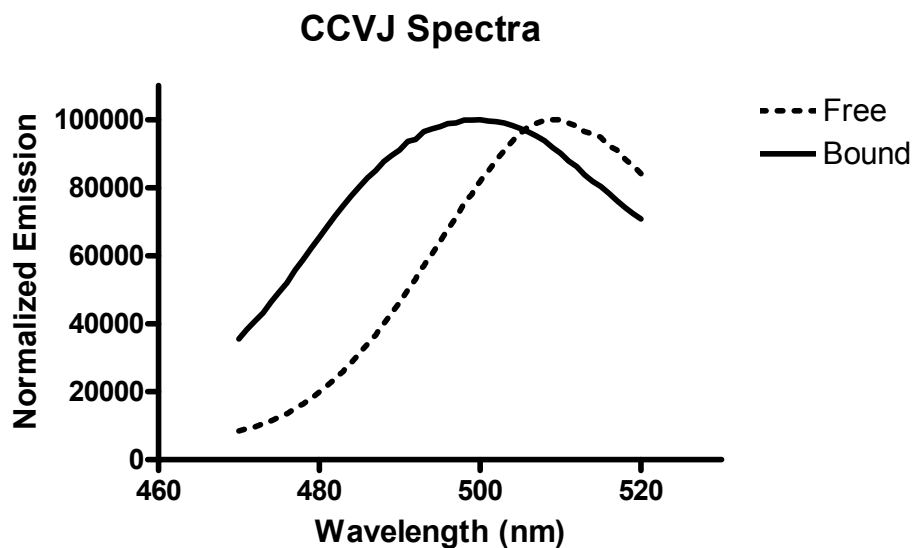
CCVJ Spectra

Figure 37: Comparison of normalized emission spectra of free and immobilized CCVJ in ethylene glycol excited at 440 nm. The emission peak for free CCVJ was 510 nm while the peak for bound was 500 nm.
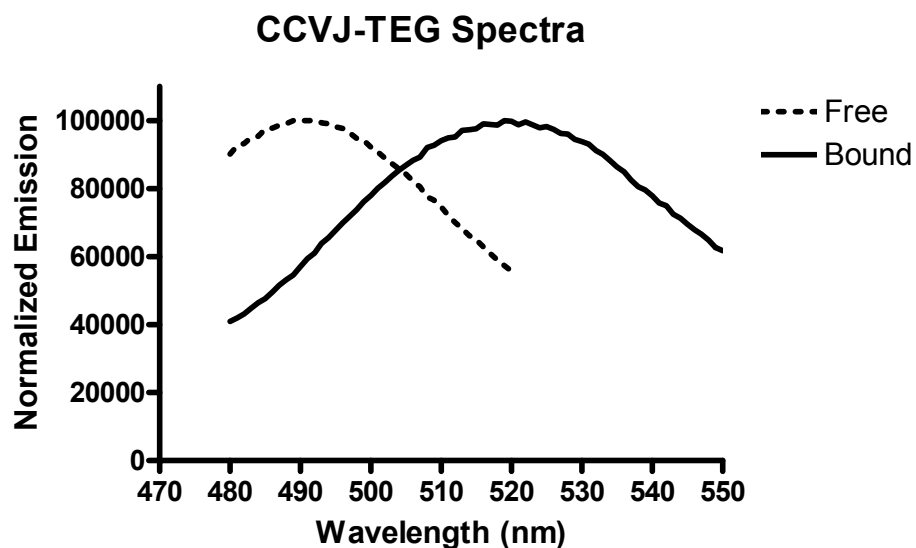
CCVJ-TEG Spectra

Figure 36: Comparison of normalized emission spectra of free and immobilized CCVJ-TEG in ethylene glycol excited at 460 nm. The emission peak for free CCVJ-TEG was 495 nm while the peak for bound was 520 nm.
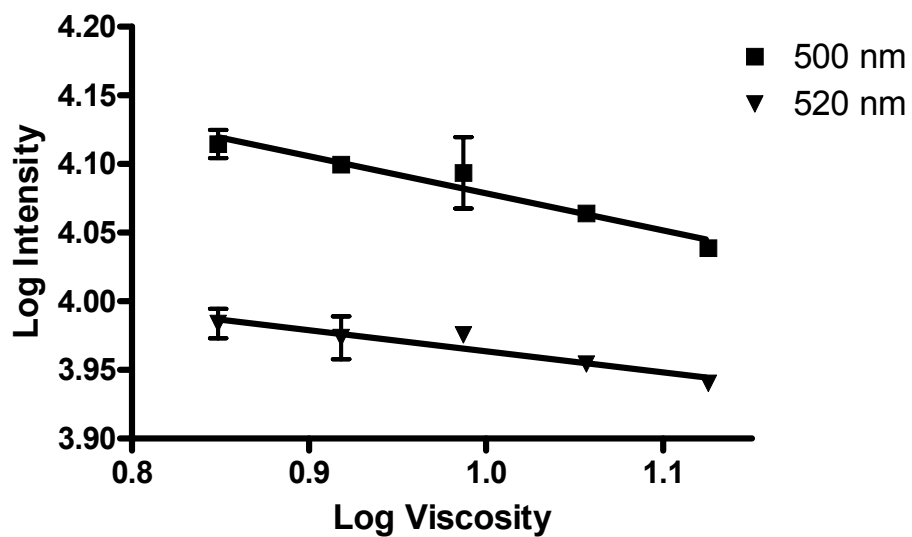
Figure 38: Unlabeled silica nanoparticles in ethylene glycol-methanol mixtures. Emission measured at 500nm and 520nm.
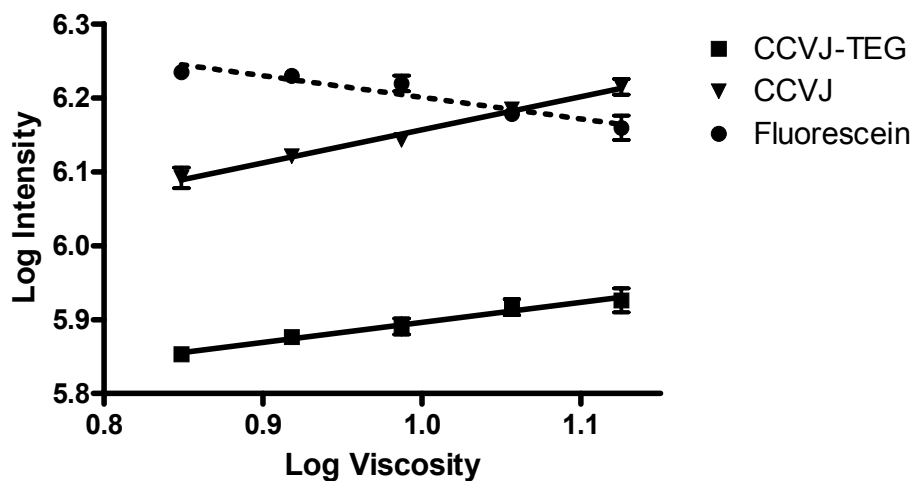
Figure 39: Comparison of log intensity to log solution viscosity of fluorescently labeled silica nanoparticles in ethylene glycol-methanol mixtures of varying viscosities.

5.5. Discussion

The intensity peaks for internal illumination were much broader than those for external illumination, which indicates significant background signal possibly from intrinsic fluorescence of fiber. The slopes of linear regression plots for internal illumination of CCVJ-labeled fibers were much less than for external illumination. The background signal associated with internal illumination is the most likely cause for its lower sensitivity. Possible disadvantages of external illumination include greater influence of sample optical properties such as refractive index and optical density. Internal illumination relies on evanescent wave excitation which is less sensitive to these properties.

Both CCVJ and CCVJ-TEG appear to retain viscosity sensitivity in ethylene glycol-methanol and ethylene glycol-glycerol mixtures after covalent surface immobilization. Refractive index correlates positively with mixture viscosity. I suspect the negative slope of the fluorescein and unlabeled samples is related to light scattering. Light scatter should decrease as the sample refractive index approaches that of glass (n=1.5). Improvement of the immobilization procedure and increased sensitivity of the immobilized molecular rotor would greatly improve the utility of this method. Nanoparticle concentration could be decreased to minimize noise from scattered light and increase measurable changes in molecular rotor fluorescence due to solvent viscosity.

Improvement of the immobilization procedure and increased sensitivity of the immobilized molecular rotor would greatly improve the sensitivity of this

method. Nanoparticle concentration could be decreased to minimize noise from scattered light and increase measurable changes in molecular rotor fluorescence due to solvent viscosity.

CCVJ-TEG normally emits near 500 nm, but immobilized emission peak is at 520 nm. This is a significant decrease in emission energy that I suspect is due to a change in the pi-bonding network. CCVJ is linked via the carboxyl group to the silane film which exposes its hydrophobic julolidine group to solvent. CCVJ-TEG is linked via single ring structure, exposing its more hydrophilic triethylene glycol moiety to the solvent.

5.6. Conclusions

This study demonstrated the feasibility of surface-immobilized molecular rotors as fluid viscosity sensors in ethylene glycol-methanol mixtures. It is my hypothesis that a more efficient molecular rotor oriented with a hydrophilic group exposed to solvent would be viscosity sensitive in aqueous solutions. The results of these experiments do not support this hypothesis, but further testing is necessary before rejecting it.

The change in Stoke's shift for the two rotors between free and bound states indicates the attachment point in the molecular structure is important for their photophysical properties. A decrease in emission energy may correlate with lower quantum yield and thus decreased signal strength, which may explain the insensitivity of the CCVJ-TEG fiber-optic probe to solution viscosity.

Fluorescent molecules typically have lower quantum yield in aqueous

97

solutions as well. An efficient molecular rotor that can be immobilized with hydrophilic parts sufficiently exposed to an aqueous environment would likely display sensitivity to the viscosity of aqueous soltuions.

CHAPTER 6.

CONCLUSION

Abnormalities in blood plasma viscosity and the corresponding endothelial wall shear stress are seen in many pathologic conditions such as diabetes mellitus, severe hemorrhage and stroke. Although viscosity and shear stress changes are not considered causes of these diseases, they can be used as markers indicating the presence, severity, and/or response to therapy, or as aids in characterizing the disease process. Although blood viscosity can be measured, it has not been fully investigated as an important factor in disease, likely because the current methods of viscosity measurement are difficult to use in clinical settings.

Instruments such as cone and plate, falling-ball, and capillary viscometers are presently being used in most fluid viscosity studies, but have several fundamental limitations in common that make them poor choices for measuring blood viscosity. Protein deposits at the instrument surface may cause erroneous readings so that meticulous cleaning of the instruments is required. An instrument that could quickly and accurately measure viscosity of small quantities of blood without applying shear would greatly benefit the study of blood rheology and its utilization in disease diagnosis and treatment.

Molecular rotors, fluorescent dyes with viscosity-dependent quantum yield [18] have previously been used to monitor polymerization [45], as sensors of protein-binding and conformation change, and as cell membrane fluidity sensors [23,25]. This work continued the investigation of molecular rotors in the role of

fluid viscosity sensors.

Hydrophilic molecular rotors were shown to be sensitive to the viscosity of aqueous colloid solutions used clinically for blood volume replacement therapy [2]. The results indicate molecular rotor fluorescence intensity changes with bulk fluid viscosity, in the presence of much larger molecules. Calibration of the method is necessary for the plasma expander used.

Fluorescence viscometry using molecular rotors was also shown to be as precise as state-of-the-art instruments currently used for fluid viscosity measurement [3]. Molecular rotors have a distinct advantage in blood plasma viscosity measurement over instruments that rely on shear stress. Blood plasma proteins adhere to instrument surfaces and form sticky layers at the air interface, making the fluid appear non-Newtonian. Viscosity measurement at low shear rates is therefore difficult. Fluorescence viscometry does not rely on shear and is well-suited for biofluid viscosity measurement.

Molecular rotor interaction with blood plasma proteins was investigated to determine what affect normal variations of protein concentration between individuals may have on fluorescence viscometry. Molecular rotors were dialyzed against individual blood plasma proteins to assess the binding affinities. The results indicate albumin is the primary protein that associates with molecular rotors. Association is dependent on molecular rotor structure. The most hydrophilic molecular rotor studied showed very low affinity for any protein. Molecular rotors that are not bound to proteins in plasma may show better sensitivity to viscosity despite variations in protein concentrations. This aspect

needs to be investigated further.

A fiber-optic viscosity probe would be very useful for remote viscosity sensing of very small sample volumes. Fluorescence can effectively be measured through an optical fiber, allowing measurement at least a meter from bulky laboratory fluorometers. Battery-powered fluorometers using fiber-optics are now feasible thanks to high intensity LEDs. Viscosity measurement in lab-on-a-chip devices may also be useful. Surface-immobilized molecular rotors were investigated for these purposes. Molecular rotors were covalently attached to the surface of glass nanoparticles and glass optical fibers. Fluorescence measurements indicate the molecular rotors retain viscosity sensitivity in non-aqueous solutions after immobilzation. Improvements in the immobilization procedure are necessary for fiber-optic probe development and for use in aqueous solutions and biofluids. The orientation of the molecular rotor with respect to the solvent must be optimized. Exposure of the hydrophilic end of the molecular rotor further into the solution may increase sensitivity. Use of a longer, rigid organosilane may also increase solvent-rotor contact. Another benefit of a fiber-optic probe is that no dye needs to be added to the sample.

REFERENCE LIST

[1] Abdel-Mottaleb, M. S. A, Loutfy, R. O., and Lapouyade, R., Non-Radiative Deactivation Channels of Molecular Rotors., *J. Photochem. and Photobiol. A:Chemistry* **48** (1989), 87-93.

[2] Akers, W. J. and Haidekker, M. A., A Molecular Rotor As Viscosity Sensor in Aqueous Colloid Solutions, *J. Biomech. Eng.* **126** (2004), 340-345.

[3] Akers, W. J. and Haidekker, M. A., Precision Assessment of Biofluid Viscosity Measurements Using Molecular Rotors, *J. Biomech. Eng.* **127** (2005), 450-454.

[4] Becker, R. C., Seminars in Thrombosis, Thrombolysis, and Vascular Biology. Part 5: Cellular Rheology and Plasma Viscosity, *Cardiology* **79** (1991), 265-270.

[5] J.B. Birks, *Photophysics of Aromatic Molecules*, Wiley-Interscience, London, 70, pp. 2-35.

[6] Boldt, J., Fluid Choice for Resuscitation of the Trauma Patient: a Review of the Physiological, Pharmacological, and Clinical Evidence, *Can. J. Anaesth.* **51** (2004), 500-513.

[7] Cao, L. K., Anderson, G. P., Ligler, F. S., and Ezzell, J., Detection of Yersinia Pestis Fraction 1 Antigen With a Fiber Optic Biosensor, *J. Clin. Microbiol.* **33** (1995), 336-341.

[8] Christmann, D. R., Crouch, S. R., Holland, J. F, and Timnick, A., Correction of Right-Angle Molecular Fluorescence Measurements for Absorption of Fluorescence Radiation., *Anal. Chem.* **52** (1980), 291-295.

[9] G.R. Cokelet, The rheology of human blood, in: *Biomechanics: Its Foundations and Objectives*, Y. Fung, N. Perrone and M. Anliker, eds, Prentice-Hall, Englewood Cliffs, NJ, 72, pp. 63-103.

[10] Dewachter, P., Laxenaire, M. C., Donner, M., Kurtz, M., and Stoltz, J. F., [In Vivo Rheologic Studies of Plasma Substitutes], *Ann. Fr. Anesth. Reanim.* **11** (1992), 516-525.

[11] Dintenfass, L., Modifications of Blood Rheology During Aging and Age-Related Pathological Conditions, *Aging (Milano.)* **1** (1989), 99-125.

[12] Doolittle, A. K., Studies in Newtonian Flow.III.The Dependence of the Viscosity of Liquids on Molecule Weight and Free Space (in Homologous Series), *J. Appl. Physiol* **23** (1952), 236-239.

[13]   Eckmann, D. M., Bowers, S., Stecker, M., and Cheung, A. T., Hematocrit, Volume Expander, Temperature, and Shear Rate Effects on Blood Viscosity, *Anesth. Analg.* **91** (2000), 539-545.

[14]   Ermondi, G., Lorenti, M., and Caron, G., Contribution of Ionization and Lipophilicity to Drug Binding to Albumin: a Preliminary Step Toward Biodistribution Prediction, *J. Med. Chem.* **47** (2004), 3949-3961.

[15]   Ernst, E. and Matrai, A., Abstention From Chronic Cigarette Smoking Normalizes Blood Rheology, *Atherosclerosis* **64** (1987), 75-77.

[16]   Ernst, E., Schmidt-Pauly, E., Muhlig, P., and Matrai, A., Blood Viscosity in Patients With Bone Fractures and Long Term Bedrest, *Br. J. Surg.* **74** (1987), 301-302.

[17]   Falipou, S., Chovelon, J. M., Martelet, C., Margonari, J., and Cathignol, D., New Use of Cyanosilane Coupling Agent for Direct Binding of Antibodies to Silica Supports. Physicochemical Characterization of Molecularly Bioengineered Layers, *Bioconjug. Chem.* **10** (1999), 346-353.

[18]   Förster, T and Hoffmann, G., Effect of Viscosity on the Fluorescence Quantum Yield of Some Dye Systems, *Z. Phys. Chem.* **75** (1971), 63-76.

[19]   J.F. Foster, Physical Properties of Amylose and Amylopectin in Solution, in: *Starch: Chemistry and Technology*, R.L. Whistler and E.F. Paschall, eds, Academic Press, New York, NY, 65, pp. 349-389.

[20]   Golden, J. P., Anderson, G. P., Rabbany, S. Y., and Ligler, F. S., An Evanescent Wave Biosensor--Part II: Fluorescent Signal Acquisition From Tapered Fiber Optic Probes, *IEEE Trans. Biomed. Eng.* **41** (1994), 585-591.

[21]   Grabowski, Z. R., Rotkiewicz, K., Siemiarczuk, A., Cowley, D. J., and Baumann, W., Twisted Intramolecular Charge Transfer States (TICT). A New Class of Excited States With a Full Charge Separation., *Nouveau Journal De Chimie* **3** (1979), 443-454.

[22]   Haidekker, M. A., Brady, T. P., Chalian, S. H., Akers, W., Lichlyter, D., and Theodorakis, E. A., Hydrophilic Molecular Rotor Derivatives - Synthesis and Characterization, *Bioorganic Chemistry* **32** (2004), 274-289.

[23]   Haidekker, M. A., L'Heureux, N., and Frangos, J. A., Fluid Shear Stress Increases Membrane Fluidity in Endothelial Cells: a Study With DCVJ Fluorescence, *Am. J. Physiol. Heart Circ. Physiol.* **278** (2000), H1401-H1406.

[24]   Haidekker, M. A., Tsai, A. G., Brady, T., Stevens, H. Y., Frangos, J. A., Theodorakis, E., and Intaglietta, M., A Novel Approach to Blood Plasma Viscosity

Measurement Using Fluorescent Molecular Rotors, *Am. J. Physiol. Heart Circ. Physiol*. **282** (2002), H1609-H1614.

[25]   Haidekker, M. A., White, C. R., and Frangos, J. A., Analysis of Temporal Shear Stress Gradients During the Onset Phase of Flow Over a Backward-Facing Step, *J. Biomech. Eng.* **123** (2001), 455-463.

[26]   H. Haljamae, Albumin: To Use or Not to Use? Contemporary Alternatives?, in: *Volume Replacement*, J.F. Baron and J. Treib, eds, Springer, Berlin, 98, pp. 1-22.

[27]   Harkness, J., The Viscosity of Human Blood Plasma; Its Measurement in Health and Disease, *Biorheology* **8** (1971), 171-193.

[28]   Healey, B. G. and Walt, D. R., Improved Fiber-Optic Chemical Sensor for Penicillin, *Anal. Chem.* **67** (1995), 4471-4476.

[29]   Hehre, E. J., Production From Sucrose of a Serologically Reactive Polysaccharide by a Sterile Bacterial Extract, *Science* **93** (1941), 237-238.

[30]   Heilmann, L., Rheological Studies on Patients With Pregnancy-Induced Hypertension (PIH), *Klin. Wochenschr..* **64** (1986), 1070-1076.

[31]   Holland, J. F, Teets, R. E., and Timnick, A., A Unique Computer Centered Instrument for Simultaneous Absorbance and Fluorescence Measurements., *Analytical Chemistry* **45** (1973), 145-153.

[32]   Iio, T., Itakura, M., Takahashi, S., and Sawada, S., 9-(Dicyanovinyl)Julolidine Binding to Bovine Brain Calmodulin, *J. Biochem.* **109** (1991), 499-502.

[33]   Iio, T., Takahashi, S., and Sawada, S., Fluorescent Molecular Rotor Binding to Actin, *J. Biochem. (Tokyo)* **113** (1993), 196-199.

[34]   Intaglietta, M., Hemodilution and Blood Substitutes, *Artif. Cells Blood Substit. Immobil. Biotechnol.* **22** (1994), 137-144.

[35]   James, E. A., Schmeltzer, K., and Ligler, F. S., Detection of Endotoxin Using an Evanescent Wave Fiber-Optic Biosensor, *Appl. Biochem. Biotechnol.* **60** (1996), 189-202.

[36]   Kato, T., Hayashi, K., Takamizawa, K., and Tsushima, N., Blood Rheology in the Endotoxin-Administered Rabbits, *Resuscitation* **23** (1992), 137-144.

[37]   Krasnoslobodtsev, A. V. and Smirnov, S. N., Effect of Water on Silanization of Silica by Trimethoxysilanes, *Langmuir* **18** (2002), 3181-3184.

[38]   Kwaan, H. C. and Bongu, A., The Hyperviscosity Syndromes, *Semin. Thromb. Hemost.* **25** (1999), 199-208.

[39]   Lakowicz, J. R., Principles of Fluorescence Spectroscopy, **2nd** (1999), 54.

[40]   Lamke, L. O. and Liljedahl, S. O., Plasma Volume Changes After Infusion of Various Plasma Expanders, *Resuscitation* **5** (1976), 93-102.

[41]   Law, K. Y., Fluorescence Probe for Microenvironments: Anomalous Viscosity Dependence of the Fluorescence Quantum Yield of P-N,N-Dialkylaminobenzylidenmalononitrile in 1-Alkanols, *Chem. Phys. Lett.* **75** (1980), 545-549.

[42]   Le Devehat, C., Khodabandehlou, T., and Vimeux, M., Impaired Hemorheological Properties in Diabetic Patients With Lower Limb Arterial Ischaemia, *Clin. Hemorheol. Microcirc.* **25** (2001), 43-48.

[43]   Letcher, R. L., Chien, S., Pickering, T. G., Sealey, J. E., and Laragh, J. H., Direct Relationship Between Blood Pressure and Blood Viscosity in Normal and Hypertensive Subjects. Role of Fibrinogen and Concentration, *Am. J. Med.* **70** (1981), 1195-1202.

[44]   B.J. Lindsey, Amino Acids and Proteins, in: *Clinical Chemistry: Principles, Procedures, Correlations*, M.L. Bishop, E.P. Fody and J.L. Duben-Engelkirk, eds, Fourth, Lippincott Williams & Wilkins, Philadelphia, 00, pp. 151-184.

[45]   Loutfy, R. O., Fluorescence Probes for Polymer Free-Volume, *Pure and Applied Chemistry* **58** (1986), 1239-1248.

[46]   Loutfy, R. O. and Arnold, B. A., Effect of Viscosity and Temperature on Torsional Relaxation of Molecular Rotors, *J. Phys. Chem.* **86** (1982), 4205-4211.

[47]   Loutfy, R. O. and Law, K. Y., Electrochemistry and Spectroscopy of Intramolecular Charge-Transfer Complexes. P-N,N-Dialkylaminobenzylidenemanononitriles, *J. Phys. Chem.* **84** (1980), 2803-2808.

[48]   Lowe, G. D., Lee, A. J., Rumley, A., Price, J. F., and Fowkes, F. G., Blood Viscosity and Risk of Cardiovascular Events: the Edinburgh Artery Study, *Br. J. Haematol.* **96** (1997), 168-173.

[49]   McGrath, M. A. and Penny, R., Paraproteinemia: Blood Hyperviscosity and Clinical Manifestations, *J. Clin.. Invest.* **58** (1976), 1155-1162.

[50]   McMillan, D. E., Further Observations on Serum Viscosity Changes in Diabetes Mellitus, *Metabolism* **31** (1982), 274-278.

[51]   Milich, K., Akers, W., and Haidekker, M., A Ratiometric Fluorophotometer for Fluorescence-Based Viscosity Measurement With Molecular Rotors., *Sensor Letters* **3** (2005), 237-243.

[52]   Nakai, D., Kumamoto, K., Sakikawa, C., Kosaka, T., and Tokui, T., Evaluation of the Protein Binding Ratio of Drugs by a Micro-Scale Ultracentrifugation Method, *J. Pharm. Sci* **93** (2004), 847-854.

[53]   Niu, C. G., Li, Z. Z., Zhang, X. B., Lin, W. Q., Shen, G. L., and Yu, R. Q., Covalently Immobilized Aminonaphthalimide As Fluorescent Carrier for the Preparation of Optical Sensors, *Anal. Bioanal. Chem.* **372** (2002), 519-524.

[54]   Otto, C., Ritter, M. M., Richter, W. O., Minkenberg, R., and Schwandt, P., Hemorrheologic Abnormalities in Defined Primary Dyslipoproteinemias With Both High and Low Atherosclerotic Risks, *Metabolism* **50** (2001), 166-170.

[55]   Perry, Robert H., Green, Don W., and Maloney, James O., Perry's Chemical Engineers' Handbook, **6th ed** (1984),

[56]   Qhobosheane, M., Santra, S., Zhang, P., and Tan, W., Biochemically Functionalized Silica Nanoparticles, *Analyst* **126** (2001), 1274-1278.

[57]   Ratzlaff, E. H., Harfmann, R. G., and Crouch, S. R., Absorption-Corrected Fiber Optic Fluorometer, *Anal. Chem.* **56** (1984), 342-347.

[58]   Reinhart, W. H., Danoff, S. J., Usami, S., and Chien, S., Rheologic Measurements on Small Samples With a New Capillary Viscometer, *J. Lab. Clin. Med.* **104** (1984), 921-931.

[59]   W. Rettig and R. Lapouyade, Fluorescence probes based on twisted intramolecular charge transfer (TICT) states and other adiabatic photoreactions., in: *Topics in Fluorescence Spectroscopy, Volume 4: Probe Design and Chemical Sensing*, J.R. Lakowicz, eds, Plenum Press, New York, 94, pp. 109-149.

[60]   Roe, P. F. and Harkness, J., Plasma Viscosity in the Elderly, *Gerontol. Clin. (Basel)* **17** (1975), 168-172.

[61]   Squire, J. R., Bull, J. P., Maycock, W., and Ricketts, C. R., Dextran: Its Properties and Use in Medicine, (1955), 8-67.

[62]   Tomiyama, Y., Brian, J. E., Jr., and Todd, M. M., Plasma Viscosity and Cerebral Blood Flow, *Am. J. Physiol. Heart Circ. Physiol.* **279** (2000), H1949-H1954.

[63]   Tsai, A. G., Friesenecker, B., McCarthy, M., Sakai, H., and Intaglietta, M., Plasma Viscosity Regulates Capillary Perfusion During Extreme Hemodilution in

Hamster Skinfold Model, *Am. J. Physiol*. **275** (1998), H2170-H2180.

 [64]   Tsai, A. G. and Intaglietta, M., High Viscosity Plasma Expanders: Volume Restitution Fluids for Lowering the Transfusion Trigger, *Biorheology* **38** (2001), 229-237.

 [65]   Wells, R., Syndromes of Hyperviscosity, *N. Engl. J. Med.* **283** (1970), 183-186.

VITA

Walter J. Akers was born December 20, 1975 in Joplin, Missouri. He graduated from Eminence High School in 1994 and was accepted as a student at the University of Missouri at Rolla. After three semesters and a change from engineering to biochemistry, he transferred to the University of Missouri-Columbia for pre-veterinary preparation. Walter was accepted by the University of Missouri College of Veterinary Medicine and began studies in the fall of 1997 and finished his Doctorate of Veterinary Medicine May of 2001. He practiced veterinary medicine in a privately-owned small animal veterinary clinic in Salem, Oregon for a year after graduation. Walter then returned to the University of Missouri-Columbia to begin a career in research. He completed a B.S. in Biochemistry in 2004 and Ph.D. in Biomedical Engineering in 2005. Walter is married to the former Renee M. Trimmer of Maitland, Missouri, and has accepted a position as Staff Scientist at the Malinckrodt Institute of Radiology at the Washington University School of Medicine, St. Louis, Missouri.